Aerosol Mass and Optical Properties, Smoke Influence on O_3, and High NO_3 Production Rates in a Western U.S. City Impacted by Wildfires

Vanessa Selimovic[1], Robert J. Yokelson[1] (iD), Gavin R. McMeeking[2] (iD), and Sarah Coefield[3]

[1]Department of Chemistry, University of Montana, Missoula, MT, USA, [2]Handix Scientific LLC, Boulder, CO, USA, [3]Missoula City-County Health Department, Missoula, MT, USA

Abstract Evaluating our understanding of smoke from wild and prescribed fires can benefit from downwind measurements that include inert tracers to test production and transport and reactive species to test chemical mechanisms. We characterized smoke from fires in coniferous forest fuels for >1,000 hr over two summers (2017 and 2018) at our Missoula, Montana, surface station and found a narrow range for key properties. $\Delta PM_{2.5}/\Delta CO$ was 0.1070 ± 0.0278 (g/g) or about half the age-independent ratios obtained at free troposphere elevations (0.2348 ± 0.0326). The average absorption Ångström exponent across both years was 1.84 ± 0.18, or about half the values available for very fresh smoke. Brown carbon (BrC) was persistent (~50% of absorption at 401 nm) in both years, despite differences in smoke age. $\Delta BC/\Delta CO$ doubled from 2017 to 2018, but the average across 2 years was within 33% of recent airborne measurements, suggesting low sampling bias among platforms. Switching from a 1.0 to a 2.5 micron cutoff increased the mass scattering and mass absorption coefficients, suggesting often overlooked supermicron particles impact the optical properties of moderately aged smoke. O_3 was elevated ~6 ppb on average over a full diurnal period when wildfire smoke was present, and smoke-associated O_3 increases were highest (~9 pbb) at night, suggesting substantial upwind production. NO_x was mostly local in origin. NO_x spurred high rates of NO_3 production, including in the presence of wildfire smoke (up to 2.44 ppb hr^{-1}) and at least one nighttime BrC secondary formation event that could have impacted next-day photochemistry.

Plain Language Summary Wildfires are complicated and difficult to sample. We characterized smoke for over 1,000 hr downwind of a large number of wildfires burning at all stages and measured species sensitive to total smoke production, the combustion characteristics, and plume evolution. The PM/CO ratio was about half that in fresh smoke, suggesting that aerosol evaporation dominates at the surface at smoke ages up to ~1–2 days. Brown carbon accounted for about half of aerosol absorption at 401 nm. O_3 levels increased significantly during smoke episodes. High NO_3 production rates were driven by local (nonfire) NO_2 sources.

1. Introduction

Biomass burning (BB) is a major source of trace gases and particulate matter (PM) that can significantly impact local, regional, and global atmospheric chemistry; air quality (AQ); climate forcing; visibility; and human health (Crutzen & Andreae, 1990; United States Environmental Protection Agency, 2016). BB is one of the largest global sources of fine organic aerosol (OA), black carbon (BC), brown carbon (BrC) (Akagi et al., 2011; Bond et al., 2004, 2013; Hecobian et al., 2010), greenhouse gases, and nonmethane organic gases (NMOG) (Yokelson et al., 2008, 2009), which are precursors for the formation of ozone (O_3) and OA. Regionally, in the western United States, wildfires produce almost twice as much $PM_{1.0}$ (particles with diameter $\leq$1.0 μm) per year as all other western aerosol sources combined (Liu et al., 2017) and frequently have large AQ impacts on extensive regions of the western United States, including urban areas.

Wildfires are also a key component of forest ecosystems with naturally occurring average frequency in the absence of human influences. However, climate change, the build-up of fuels due to fire suppression, and the expansion of the wildland-urban interface (WUI) have led to increased fire risk and fire behavior that is more difficult to control (Schoennagel et al., 2017; Shivdenko & Schepaschenko, 2013; Stevens et al., 2014; Turner et al., 2019). While globally, the length of fire season has increased by ~19% from 1979 to 2013, the increase in fire season has been even greater in the western United States (Jolly et al., 2015) and has been

closely tied to temperature, drought, and anthropogenic climate change (Abatzoglou & Williams, 2016; Marlon et al., 2012; Westerling et al., 2006). Aggressive fire suppression techniques have also led to an accumulation of fuels in drier forests previously adapted to frequent low-severity fires that reduced less fire-resistant vegetation. The fuel build-up in these dry forests drives more intense fires and, potentially, conversion into nonforest ecosystems. In some moister forests adapted to long fire return intervals, the conditions for major fire activity appear to be occurring with greatly increased frequency due to anthropogenic climate change (Turner et al., 2019). The expansion of the WUI increases wildfire threats to people, homes, and infrastructure and fundamentally changes the tactics and cost of fire suppression; these issues can account for as much as 95% of fire suppression costs (United States Department of Agriculture, 2015). Prescribed fires and reducing aggressive fire suppression techniques are options to remedy the situation. In particular, combining fuel consumption and emission factor (EF) data suggests that prescribed fires produce about 18 times less PM pollution per unit area burned than wildfires (Liu et al., 2017; section 4.4). Prescribed fires can reduce hazardous fuels under safe conditions when smoke is largely directed away from most populated areas, and they are a major, successful component of land management in the southeast United States. However, recent research suggests that in the western United States more prescribed fire can reduce wildfire pollution increases and benefit safety in the WUI but not enough prescribed burning can be done to eliminate future increases in wildfire pollution (Schoennagel et al., 2017). Due to expected wildfire increases and to guide the recommended increased implementation of prescribed fires, robust models of smoke production, transport, and chemistry are increasingly needed to understand the impacts of all fires on AQ, visibility, and climate.

Modeling fire and smoke physics is challenging, especially for wildfires. Wildfires can burn day and night (Saide et al., 2015; Vermote et al., 2009) for months in complex and variable fuels emitting smoke from multiple, rapidly changing locations with injection altitudes ranging over time from downslope flow (Bertschi et al., 2003) to the lower stratosphere (Fromm et al., 2000; Herron-Thorpe et al., 2014; Stocks et al., 1996). Complex downwind terrain influences transport winds and traps smoke (Wagenbrenner et al., 2016). Emissions are thus subjected to a wide range of dispersion scenarios including injection into the upper troposphere or lower stratosphere with or without pyrocloud formation (Peterson et al., 2017), persistent widespread regional boundary layer haze (Chen et al., 2017), downslope flow of poorly lofted residual smoldering combustion emissions (Selimovic et al., 2019), entrapment under nighttime-early morning inversions in mountain valleys (Ferguson et al., 2003), fast dilution of point sources in the (warmer, wetter) boundary layer, slower dilution of area sources or in the (colder and dryer) free troposphere (Hodshire et al., 2019), and midday mixing down of elevated polluted layers (Xu et al., 2018).

Modeling smoke chemistry is also challenging; the chemical composition of freshly emitted smoke may change as fuels or combustion conditions change (Hatch et al., 2017, 2018; Jen et al., 2019). Smoke evolution is also complex and highly dependent on variable atmospheric processing scenarios, but an important suite of smoke species is linked by a connection to UV light. BrC is a current research focus that impacts climate and UV photochemistry. UV light impacts the lifetime of BrC (Fleming et al., 2020), which competes for UV photons with gases like HONO and NO_2, thereby altering photochemistry. UV photolysis of NO_2 is a source of O_3 and NO_2 reacts with O_3 to form NO_3, which may react with NMOG to make BrC and secondary OA (SOA) in general, but O_3 and OH are also important oxidants that can generate BrC and SOA. The amount of NMOG precursors is impacted by gas-particle partitioning, which depends on dilution (May et al., 2013; Robinson et al., 2007), and the emissions of NMOG are higher when the smoldering/flaming ratio increases (Burling et al., 2011). The smoldering/flaming ratio was observed to be higher at night than during the day in one study (Benedict et al., 2017), and lab-simulated fires indicate that BrC emissions are strongly associated with smoldering combustion (Selimovic et al., 2018). NO_2 is produced by flaming combustion or can be from local sources downwind. O_3 is abundant in background air and made during the daytime in smoke plumes (Akagi et al., 2012, 2013). Secondary nighttime formation of BrC from reactions of fire-emitted NMOGs with NO_3, and potentially O_3 or other pathways, is likely. Stockwell et al. (2015) showed that smoldering combustion of biomass releases large amounts of monoterpenes, furans, cresol, and so forth, all of which can react quickly with NO_3 and form UV-absorbing organic nitrates that have potential to become condensed phase chromophores (BrC) as eventual products (Brown et al., 2013), and observations of nighttime smoke impacting the Colorado Front Range also showed high levels of these same precursors (Gilman et al., 2015).

Further, OA in BB plumes intercepted at Mt. Bachelor Observatory was more oxidized after nighttime aging (Zhou et al., 2017). A significant amount of uncertainty in isolating and evaluating the optical properties of BrC and its overall radiative impact remains difficult to accurately assess, as BrC emissions are typically mixed with coemitted BC and nonabsorbing OA, which can result in some measurement difficulties (Pokhrel et al., 2017; Wang et al., 2017). Nonetheless, several studies have found that including BrC in climate models suggests that net radiative forcing of BB would move in a positive direction (Ervens et al., 2011; Feng et al., 2013; Forrister et al., 2015; Graber & Rudich, 2006; Jacobson, 2014; Laskin et al., 2015; Saleh et al., 2014; Wang et al., 2014, 2017; Zhang et al., 2020). This has important climate implications, especially in association with warming-induced increases in fire activity (Bowman et al., 2017; Doerr & Santín, 2016; Feng et al., 2013; Westerling et al., 2006). Other important smoke evolution issues include the net result of competition between OA evaporation and SOA formation as well as the impact of smoke on surface O_3 levels. Airborne and laboratory studies of SOA and lab studies of BrC evolution so far provide variable outcomes and no clear guidance on the factors controlling smoke evolution (Ahern et al., 2019; Cubison et al., 2011; Fleming et al., 2020; Garofalo et al., 2019; Tkacik et al., 2017; Vakkari et al., 2018; Yokelson et al., 2009).

Airborne studies have successfully provided initial, near source emissions and the first few hours of plume evolution at high altitude in vigorously lofted plumes (Akagi et al., 2012, 2013; Collier et al., 2016; Garofalo et al., 2019; Liu et al., 2017; Sedlacek et al., 2018; Yokelson et al., 2009), but they rarely provide specific or typical smoke characteristics in heavily impacted surface locations, which are needed to evaluate model predictions of surface AQ. Surface measurements downwind of the source, especially in valleys at low elevations, can document specific and typical smoke air-quality characteristics in populated areas. Ground-based measurements can also provide a top-down evaluation of net regional surface impacts using ratios between inert tracers such as BC and carbon monoxide (CO) ($\Delta BC/\Delta CO$) sensitive to the flaming/smoldering ratio at the source, ratios including evolving species (e.g., $\Delta O_3/\Delta CO$, $\Delta PM/\Delta CO$, and $\Delta BrC/\Delta CO$) sensitive to secondary O_3/aerosol evolution, and time series or hourly average values for inert tracers (e.g., BC and CO) sensitive to assumed emissions production and assumed diurnal profiles of fuel consumption as well as meteorology. Thus, constraining these variables is critical to accurately assessing climate and AQ impacts especially as they relate to model simulation of smoke downwind in populated areas. Such surface measurements, which are also needed to understand the interaction of regional smoke with non-BB sources, are still relatively rare (Braun et al., 2017; McClure & Jaffe, 2018; Selimovic et al., 2019).

To address the above issues, we began measurements of wildfire smoke impacting the Missoula valley (a western urban center downwind of numerous wildfires) in August–September 2017 obtaining 500 hr of data (Selimovic et al., 2019). In this study we continued the measurements, with an expanded suite of instruments, for another 517 hr of smoke impacts during August–September 2018. Two photoacoustic extinctiometers (PAXs), a Fourier-transform-infrared spectrometer (FTIR) and, added in 2018, an O_3 monitor, a NO_x monitor, and a second FTIR were used to characterize the smoke that entered the valley. A Montana Department of Environmental Quality (DEQ) BAM 1020 measured $PM_{2.5}$ (PM $\leq$2.5 µm in diameter). The PAXs provided measurements of scattering and absorption at two wavelengths (401 and 870 nm), BC mass, contributions to UV absorption nominally due to BrC, and derivations of the single scattering albedo (SSA), absorption Ångström exponent (AAE), and scattering Ångström exponent (SAE). The optical property measurements can be normalized to the aerosol mass data to probe multistep, bottom-up calculations of climate-relevant aerosol optical properties that start with aerosol mass. Further, combining CO measured by our FTIRs with the other species measured (BC and $PM_{2.5}$) produced ratios relevant to models, as mentioned above. Finally, we measured smoke impacts on O_3, and combining our NO_2 and O_3 measurements allowed us to calculate the NO_3 production rate and probe the potential NO_3 contribution to in situ nighttime BrC formation. The main goals of our study are to assess the relevance of lab and airborne field measurements, the representativeness of emissions inventories, and guide model development by documenting actual surface level characteristics of aged/transported wildfire smoke in a representative, regional population center. We also interpret and assess the interannual variability of our results by comparing 2018 to our previous (2017) measurements of ambient smoke in the Missoula valley (Selimovic et al., 2019).

2. Materials and Methods

2.1. Site Descriptions

Our smoke monitoring sites in Missoula, MT, remained unchanged between 2017 and 2018, and they are described in more detail in Selimovic et al. (2019). We reiterate a few key details here. Trace gases and particles were measured through colocated inlets at the University of Montana (UM), ~12.5 m above the ground through the window of our laboratory on the top floor of the Charles H. Clapp building (CHCB), which is ~1.1 km from the nearest road that gets significant traffic during summer recess (http://map.umt.edu/#17/46.85920/-113.98335). $PM_{2.5}$ measurements were made by the Montana DEQ via a stationary $PM_{2.5}$ monitor located in Boyd Park, Missoula, ~3.2 km southwest of the CHCB, with both sites being located in the Missoula valley proper. Missoula is located ~800 km from the nearest large cities deep within an extensive, lightly populated to unpopulated region containing few anthropogenic sources. Missoula and the surrounding region are occasionally impacted by prescribed fires and more frequently by summer wildfires, which can be numerous (https://www.nifc.gov/fireInfo/fireInfo_statistics.html).

2.2. Instrument Details

2.2.1. Fourier Transform Infrared Spectrometers

Measurements of CO were made using two colocated FTIRs. The first FTIR (Midac Corp., Westfield, MA), used during the 2017 smoke measurements, is described in detail elsewhere (Selimovic et al., 2019). The second FTIR, added during the 2018 monitoring period, consists of a Bruker Matrix-M IR Cube spectrometer with an MCT Stirling cycle cooled detector interfaced to a permanently aligned 78 m closed uncoated multipass White cell (IR Analysis, Inc.) that is more sensitive due to the longer path length. Ambient air was drawn into both systems at ~6 L min^{-1} via a downstream IDP-3 dry scroll vacuum (Agilent Technologies) pump using two respective 0.635 o.d. corrugated Teflon inlets colocated with the other inlets. Spectra for both FTIRs were collected at a resolution of 0.50 cm^{-1}. A time resolution of approximately 5 min was more than adequate for both systems, and sensitivity was increased by coadding scans at their respective frequencies. Although the systems were designed for source measurements and are described elsewhere in more detail (Akagi et al., 2013; Selimovic et al., 2019; Stockwell, Christian, et al., 2016; Stockwell, Jayarathne, et al., 2016), both FTIRs are convenient for ambient monitoring because the Stirling cooled detectors do not require refilling of liquid nitrogen allowing mostly autonomous operation. Additionally, the use of two FTIRs allowed for intercomparison of trace gas measurements and served to supplement data in instances where it might have been missing from the other system (i.e., if one system shut down unexpectedly). Although both FTIRs can measure an extensive range of trace gases from sources, in the relatively dilute smoke impacting Missoula during 2018, most gases were retrieved with insufficient signal to noise or influenced by too many sources (e.g., CH_4 and CO_2) to be readily interpretable; thus, only CO is reported. To summarize in context, in 2017 many of the wildfires were close to Missoula, CO levels reached almost 3,000 ppb, and a number of gases (such as ethylene, ammonia, and methanol) were often above the FTIR detection limits of several ppb. In 2018, the wildfires were further from Missoula, CO levels remained below ~800 ppb, and, of the FTIR gases, only excess CO was measured with sufficient enhancement to clearly dominate background variability. CO mixing ratios were quantified by fitting a region of the mid-IR transmission spectra with a synthetic calibration nonlinear least squares method (Griffith, 1996; Yokelson et al., 2007) applying the HITRAN spectral database (Rothman et al., 2009). Excess CO was virtually identical on the two systems. Uncertainties in excess CO mixing ratios in smoke (ppmv) varied by spectrum and were dominated by uncertainty in the reference data (<%) and the background (~5–20 ppb).

2.2.2. Ozone Monitor

The 2B Technologies (Boulder, CO) Model 211 O_3 monitor is a dual-beamed 254 nm photometer that uses the reaction between ambient O_3 and NO generated in situ by upstream photolysis of added nitrous oxide (N_2O) to quantify ozone by conventional UV photometry without the issues affecting conventional O_3 scrubbers. Light intensity measurements are made with O_3 present (I) and with O_3 selectively removed by NO (I_0), and the O_3 concentration is then calculated using the Beer-Lambert law. O_3 calibrations were run using a model 306 O_3 calibrator (Birks, Andersen, et al., 2018, 2B Technologies). Some UV-absorption O_3 monitors remove O_3 by passing the sample air flow through a solid scrubber, which ideally would destroy O_3 but pass mercury and any UV-absorbing compounds. In practice, however, mercury and aromatic compounds such as benzene, toluene, and xylene can adsorb or react at the solid-phase scrubber surface. As a result,

traditional O_3 monitors may report erroneously high O_3 values by up to a few ppb in some cases (2B Technologies, https://twobtech.com/docs/tech_notes/TN040.pdf). A 2 L min^{-1} sample flow of ambient air was drawn into the instrument through a 0.638 cm o.d. FEP inlet (~12.5 m above ground level) and a Teflon filter (Savillex, 47 mm 5–6 micron) to remove particles, which was replaced every 2 weeks or when visual signs of filter loading were apparent. O_3 was sampled at 1 min intervals, but the data were averaged to 5 min for final analysis to match the time resolution of the FTIRs. Resolution of the 211 O_3 monitor is 0.1 ppb, with a limit of detection (2σ) of 1.0 ppb for a 10 s average.

2.2.3. NOx Monitor

The 2B Technologies model 405 nm NO_x monitor measures nitrogen dioxide (NO_2) directly by absorbance at 405 nm and nitric oxide (NO) after conversion to NO_2 with ~100% efficiency using the reaction of NO with O_3. Because NO_2 has a lower absorption cross section than O_3, a folded cell with corner mirrors is used to produce a long absorbance path of ~2 m to achieve approximately similar sensitives for NO_2 as for ozone (Birks, Williford, et al., 2018). Sample air is continuously drawn through the instrument by an internal pump at a flow rate of ~1.5 L min^{-1} through 0.638 cm o.d. FEP tubing colocated with the other inlets and a Teflon filter (Savillex, 47 mm 5–6 micron) to remove particles. The filter was replaced every ~2 weeks or when visual signs of filter loading were apparent. The instrument was "zeroed" on multiple occasions using zero air that was humidified to match ambient RH with nafion tubing. This ensures the refractive index in the cell and the path length do not change. The measurement of light intensity in the absence (I_0) and presence (I) of NO_2 allows the NO_2 concentration to be calculated using the Beer-Lambert law. NO is quantified by measuring the decrease in light intensity while adding O_3 to convert NO to NO_2. A small, ~1–2%, loss of 405 nm absorbance from the reaction of NO_2 with O_3 is corrected in the firmware (Birks, Williford, et al., 2018). NO_2, NO, and NO_x were measured/logged at 1 min time resolution, but the data were averaged to 5 min for final analysis to match the time resolution of the FTIRs, and NO and NO_2 were corrected for small zero offsets (~2 ppb average). NO_x was recalculated from corrected NO and NO_2. Accuracy of the NO_x monitor was limited primarily by the drift in manual zeros of 0.75 ppb with total uncertainty in 5-min NO_x data being ~2 ppb (1σ).

2.2.4. PAXs at 870 and 401 Nm

Particle absorption and scattering coefficients (B_{abs}, Mm^{-1}, B_{scat}, Mm^{-1}) were measured directly at 1 s time resolution using two PAXs (Droplet Measurement Technologies, Inc., Longmont, CO; Lewis et al., 2008; Nakayama et al., 2015), which were then used to derive the SSA at 401 and 870 nm and the AAE and SAE. Details for calculating SSA and AAE, as well as operation and limitations of the PAX instrumentation, are described in detail elsewhere (Selimovic et al., 2019), but we reiterate a few key points for the 2018 monitoring period. The main PAX sample line was 0.638 cm (o.d.) Cu tubing colocated with the other inlets. A 1 L min^{-1} aerosol sample flow was drawn through each PAX using a downstream IDP-3 scroll vacuum pump (Agilent Technologies). A scrubber and dryer removed absorbing gases and kept relative humidity below 30%, as described in detail by Selimovic et al., 2019. The 1 Hz PAX data were averaged to 5 min and matched the time resolution used for the other instruments. In 2018, we switched from a 1.0 μm cutoff cyclone to 2.5 μm cyclone.

We directly measured aerosol absorption (B_{abs}, Mm^{-1}) and calculated BC concentration (μg m^{-3}) at ambient temperature and pressure using the literature and manufacturer-recommended mass absorption coefficient (MAC) for pure BC (4.74 ± 0.63 m^2 g^{-1} at 870 nm) (Bond & Bergstrom, 2006), but note that the BC mass can be adjusted using a different MAC value. To a good approximation, sp^2-hybridized carbon (including BC) absorbs light proportional to frequency (Bond & Bergstrom, 2006). Thus, the B_{abs} contribution from BC at 401 nm can be derived from ~2.17 times B_{abs} at 870 nm (assuming an AAE of one, negligible BrC absorption at 870 nm, and minimal lensing effects). Any additional B_{abs} at 401 nm can be assigned to BrC (B_{abs}, BrC) with this attribution subject to limitations discussed elsewhere (Lack & Cappa, 2010; Lack & Langridge, 2013; Lack et al., 2008; Pokhrel et al., 2016, 2017; Subramanian et al., 2007).

Uncertainty in PAX absorption and scattering measurements has been estimated to be ~4–11% (Nakayama et al., 2015), and 5 min noise in scattering and absorption for the 870 nm instrument were 5 and <1 Mm^{-1}, respectively, while 5 min noise in scattering and absorption for the 401 nm instrument were 20 and <1 Mm^{-1}, respectively. However, a few sources of uncertainty, for instance, MAC increases due to coatings, particle losses in the dryer or scrubber, and truncation error in the nephelometer, may all contribute. Mie calculations suggest scattering could be underestimated by 1% at 870 nm and 2.5% at
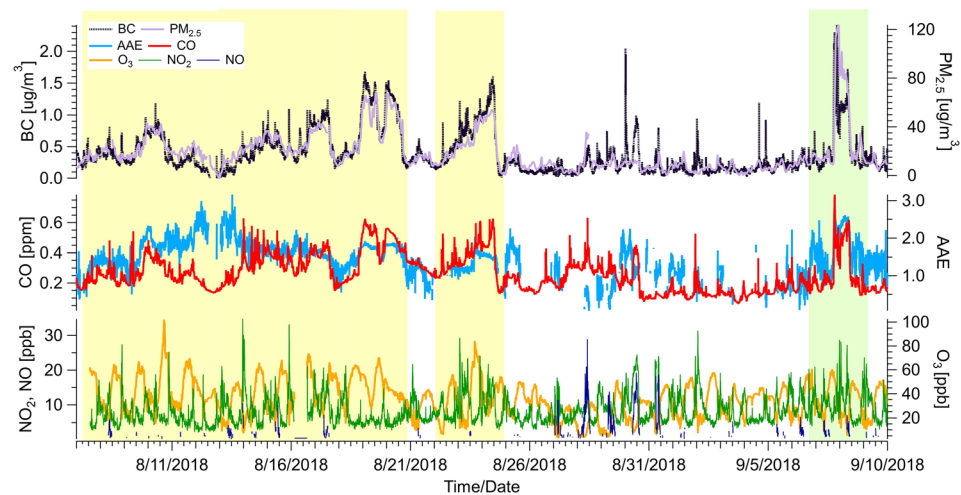
Figure 1. Time series of hourly PM, hourly derived AAE, 5-min BC, CO, NO_x, and O_3 measurements from Missoula. Sections shaded in yellow represent wildfire smoke-impacted periods. Sections shaded in green represent prescribed fire smoke-impacted periods. Unshaded areas represent anthropogenic impacts and were not included in the analysis.

401 nm due to truncation error. This would reduce mass scattering coefficients (MSCs; $m^2 g^{-1}$) (section 4.6), and typically a 1% reduction in scattering would imply approximately a tenth of a percent of value underestimation in SSA. Particle losses would reduce scattering, absorption, and derived BC but have no impact on SSA, SAE, or AAE. We found that adding an extra scrubber reduced scattering and absorption at both wavelengths by $7 \pm 5\%$ on average and adjusted the data upward by 13% to account for both the dryer and scrubber (Selimovic et al., 2019). Unlike particle losses, an increased MAC due to "lensing," mentioned above, could inflate BC values by up to ~30% (Pokhrel et al., 2017).

2.2.5. Montana DEQ $PM_{2.5}$

The Montana DEQ uses beta attenuation monitors (Met One Instruments, Model BAM-1020) in accordance with U.S. EPA Federal Equivalent Methods (FEMs) for continuous $PM_{2.5}$ monitoring, which is described in more detail in Selimovic et al. (2019). Critically, however, combining $PM_{2.5}$ measurements with our scattering and absorption measurements from the PAX allows us to derive values for MAC and MSC at both wavelengths, which is discussed more in section 4.6. Current and archived AQ data for the state of Montana can be accessed online (using the following link: http://svc.mt.gov/deq/todaysair/). We attempted to be precise about $PM_{1.0}$ and $PM_{2.5}$ when comparing measurements, but also note that $PM_{1.0}$ is usually about 80% of $PM_{2.5}$ (Reid et al., 2005), and so in some cases when a statement is true for both sizes, we may indicate that by using the general term PM.

2.2.6. Emission Ratios and Downwind Enhancement Ratios

We used the time series of our mixing ratios or concentrations for each analyte measured to derive other values that are broadly useful for both study comparisons and integration in local to global chemistry and climate models. In order to do this, we produced emission ratios (ERs) and enhancement ratios. The calculation of these two types of ratios is identical, but an ER is only the appropriate term for a ratio measured directly at a single source or further downwind for relatively inert species such as BC and CO. An excess amount, denoted by "ΔX" for each species X, is calculated for all species measured by subtracting the comparatively small background based on a sloping baseline from the first to the last point of a smoke impact. Then, for example, the ratio for each species relative to CO ($\Delta X/\Delta CO$) is the ratio between the sum of ΔX over the entire smoke-impacted period relative to the sum of ΔCO over the entire smoke-impacted period. Mass ratios to CO were calculated for BC and $PM_{2.5}$ with enhancement of hourly $PM_{2.5}$ above 12.5 $\mu g/m^3$ used to define the time limits for each smoke-impacted period as discussed further in sections 3 and 4.1.

3. Overview of Smoke Impacts

Figure 1 shows the hourly average concentrations for $PM_{2.5}$, AAE derived from 5-min averages of B_{abs} at 401 and 870 nm, and 5-min average concentrations or mixing ratios of BC, CO, NO_x, and O_3 from 7 August to 10

September 2018. Most of the summer was characterized by AQ classified as "good" by the US EPA ($<12.5\,\mu g/m^3$ of $PM_{2.5}$) and clear visibility of mountains up to 80 km distant. As shown in more detail in Figures S1–S5 in the supporting information, smoke from wildfires and one prescribed fire contributed to episodes lasting for ~1–4 days during which hourly $PM_{2.5}$ ranged as high as $120\,\mu g/m^3$ ("unhealthy," U.S. EPA), distant mountains "disappeared," and nearby mountains were partially obscured (Figure S6). In Figure 1, wildfire smoke episodes are represented by the yellow shaded area and were identified by sustained periods (≥ 6 hr) when hourly $PM_{2.5}$ was elevated above the $12.5\,\mu g\,m^{-3}$ EPA standard for "good" AQ and smoke was visibly present. Episodes started at the first point elevated above the cutoff and ended at the last elevated point before a sustained clean period or a wind shift bringing smoke from a new direction started a new event. Wildfire smoke episodes also had large simultaneous enhancements in CO and BC. High correlation of CO and BC to $PM_{2.5}$ suggests that the smoke was well mixed on the spatial scale that separated the $PM_{2.5}$ and UM equipment (Figures S7–S11). In contrast, anthropogenic pollution (26 August to 5 September) is confidently identified and differentiated from smoke because it presents as much briefer spikes in CO or NO_x without sustained impacts on both regional visibility or the $PM_{2.5}$ monitor several km distant.

To investigate the wildfire sources contributing to each episode, we used a combination of meteorological observations, geostationary satellite observations, near-surface smoke according to the High Resolution Rapid Refresh (HRRR) model (https://rapidrefresh.noaa.gov/hrrr/), and back trajectory calculations utilizing the National Oceanic and Atmospheric Administration (NOAA) Air Resources Laboratory Hybrid Single Particle Lagrangian Integrated Trajectory (HYSPLIT; Draxler, 1999; Draxler & Hess, 1997, 1998; Stein et al., 2015). For wildfires, the fact that multiple fires at different distances upwind (~150–800 km) could simultaneously impact Missoula, the long duration of the impacts, variable winds over the duration, and complex topography and micrometeorology made precise smoke ages difficult to assign or even inappropriate. An "age spectrum" may be a more fitting concept. We characterize the wildfire smoke as "up to several days old" with 20 ± 10 hr (1σ) being a rough best guess at average age in 2018. Figures S1–S5 provide our best guess at the source region for each smoke episode. The situation in 2017 was similarly complex, but much more of the Missoula smoke in 2017 was from wildfires <100 km distant (see map at https://www.atmos-chem-phys-discuss.net/acp-2018-1063/acp-2018-1063-AC3-supplement.pdf). Thus, an age characterizing most of the smoke could sometimes be estimated in 2017, and the 2017 smoke was clearly younger and more concentrated on average in 2017 (hourly $PM_{2.5}$ up to $471\,\mu g/m^3$) than 2018 (Selimovic et al., 2019).

We also present measurements for one 2018 "summer" prescribed fire impact (shaded in green). The prescribed fire was a well-documented, isolated event, and the exact location was known allowing a reliable estimate of smoke age as ~3 hr old. The prescribed fire burned over 100 ha, in a Lodgepole pine dominated ecosystem, and was a stand-replacing fire, producing smoke likely more similar to that from naturally occurring wildfires than is the case for the more common lower-intensity spring or fall prescribed fires that focus on clearing out understory fuels while preserving overstory trees.

4. Results and Discussion

4.1. O$_3$

Numerous airborne studies have documented O_3 formation in smoke plumes (Akagi et al., 2013; Liu et al., 2016), and several studies have suggested that wildfires can also lead to an increase in the amount of ground-level O_3 (Brey & Fischer, 2016; Liu et al., 2016; Morris et al., 2006). For instance, wildfire emissions enhanced average summertime monthly mean O_3 by 2–8 ppb in the Intermountain West (Jaffe et al., 2013, 2018). In another study boundary layer O_3 showed more influence from local, continental, or marine sources, while observations at high-elevation sites (1.5–3.0 km above sea level) showed greater influence from large-scale downward mixing of free tropospheric air and from transport of photochemically aged plumes from wildfires (Ambrose et al., 2011). In general, the total amount of O_3 in an area is a complex combination of the relative amounts of NMOGs and NO_x, meteorological conditions supporting local production, and the amount of O_3 present in background/transported air (Lindaas et al., 2017). In this section we investigate the effect of both dilute, aged (up to several days) wildfire smoke, and thicker, moderately fresh (~3 hr old) prescribed fire smoke on O_3 levels in Missoula by comparing the amount of O_3 present in typical conditions during clear-sky to smoke-impacted days.
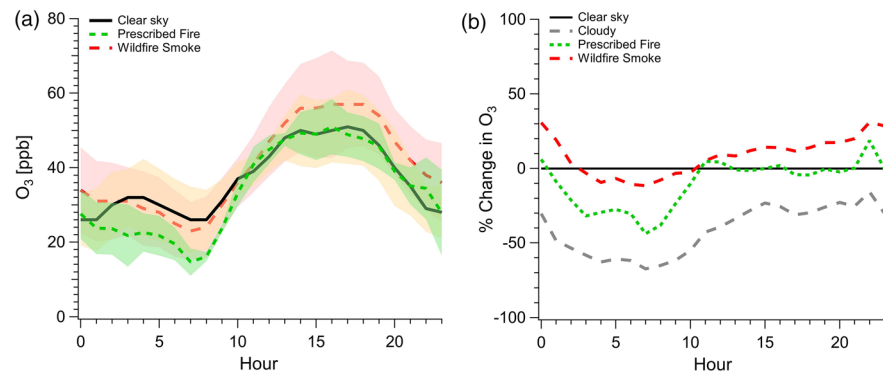
Figure 2. (a) A comparison of the 2018 average diurnal cycle of O_3 during clear-sky, wildfire (aged, up to several days) smoke-impacted periods and prescribed (3 hr old) smoke-impacted periods. Shaded area in yellow represents $\pm 1\sigma$ for clear-sky background values. Shaded area in green represents $\pm 1\sigma$ for prescribed fire smoke values. Shaded area in red represents $\pm 1\sigma$ for wildfire smoke values. (b) Percent change relative to the average diurnal cycle of O_3 during wildfire smoke-impacted, prescribed fire smoke-impacted, and cloudy days.

The two largest mixing ratios in our 5-min O_3 data are associated with aged smoke from Idaho (102 ppb; Figure S1) and Washington (82 ppb; Figure S4). O_3 values associated with aged smoke from Idaho occurred during higher than normal daily maximum temperatures (38°C), but the O_3 values associated with aged Washington smoke were in cooler air in comparison (25°C). Although higher temperatures are associated with higher O_3 values, the fact that these peaks are about 45 and 25 ppb higher, respectively, than the typical summertime 5-min O_3 maximum in clean air suggests that aged smoke (and the meteorological conditions that favor smoke production) can be associated with significant enhancements in O_3 exposure. To explore this systematically, we used hourly average O_3 data. Diurnal cycles for O_3 in each case are plotted in Figure 2a and were compiled by computing hourly averages from 5 min O_3 data, for each hour of the day over the duration of the study.

To facilitate discussion, we divided the study data into four categories with the average daily $PM_{2.5}$ and temperature and their 1σ variation given for each category in parentheses. "Clear" days ($6.8 \pm 1.9\ \mu g\ m^{-3}$, $19 \pm 3.6°C$) and "cloudy" days ($7.2 \pm 2.2\ \mu g\ m^{-3}$, $14 \pm 2.3°C$) were verified using historical weather data (https://www.wunderground.com/history/) and satellite retrievals (http://rammb-slider.cira.colostate.edu/) and had good AQ with $PM_{2.5} \leq 12.5\ \mu g\ m^{-3}$. "Wildfire" ($26 \pm 16.5\ \mu g\ m^{-3}$, $21 \pm 3.3°C$) and "prescribed fire" days ($87\ \mu g/m^3$, $20°C$) had $PM_{2.5} > 12.5\ \mu g/m^3$ due to these fire types, respectively. Although we acknowledge that O_3 exhibits a temperature dependence and typical concentrations vary seasonally, on clear days hourly-average O_3 mixing ratios remained fairly consistent around 50 ± 5 ppb during the afternoon and 30 ± 5 ppb at night throughout the monitoring period. Figure 2a shows increases in O_3 diurnal cycle mixing ratios throughout most periods of the day during wildfire smoke-impacted times, compared to the average clear-sky diurnal cycle. The O_3 mixing ratio averaged over the whole of the diurnal cycle was, on average, ~6 ppb (15%) higher during wildfire smoke-impacted periods than during clear-sky periods. Conversely, the O_3 mixing ratio averaged over the whole of the diurnal cycle was on average ~4% lower during the prescribed fire period than clear sky conditions, most likely due to reduced photochemical production associated with high $PM_{2.5}$ and BrC levels (Baylon et al., 2018) in the less-diluted and less-aged smoke from this comparatively close-by fire. McClure and Jaffe (2018) observed a consistent pattern in Boise, ID in summer 2017 where smoke enhanced O_3 up to 60–70 $\mu g\ m^{-3}$ $PM_{2.5}$ but reduced O_3 at higher $PM_{2.5}$ levels. In Missoula in 2018, we observe the largest relative enhancements of O_3 during aged, wildfire smoke-impacted periods after sunset and persisting for several hours after midnight with the mixing ratio of O_3 on average, ~9 ppb (23%) higher than corresponding average clear-sky periods. This suggests that aged smoke could prolong the O_3 lifetime in the dark or that wildfire smoke enhanced daytime O_3 formation upwind of Missoula more than in Missoula, and these air masses arrived in Missoula after dark, with the latter case implying substantial regional enhancement in O_3 due to wildfire smoke.
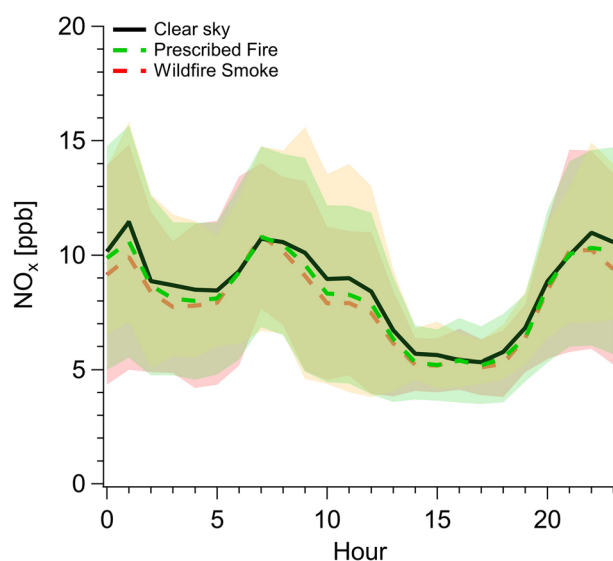
Figure 3. Average hourly diurnal cycles of NO_x measured in the Missoula valley calculated from 1 hr averages of 5-min data. Shaded area in yellow represents $\pm 1\sigma$ for background values. Shaded area in green represents $\pm 1\sigma$ for prescribed fire smoke values. Shaded area in red represents $\pm 1\sigma$ for wildfire smoke values.

Smoke evolution was studied in isolated BB plumes by combining field observations during the Southeast Nexus (SENEX) campaign with chemical box modeling using laboratory derived BB EFs measured as part of the Fire Influence on Global and Regional Environments (FIREX) campaign (Koss et al., 2018; Selimovic et al., 2018). The model of Decker et al. (2019) showed that although a change in the ambient concentration of O_3 has little effect on the relative reactivity of nighttime oxidants such as NO_3 and O_3, including nighttime O_3 oxidation in photochemical models should still be critical, as it has potential to affect next-day photochemistry. For instance, Decker et al. (2019) reported that while the nighttime oxidation of NMOGs produced by BB for some fuels is dominated by NO_3, in some cases, oxidation by O_3 remains significant (e.g., 43% for ponderosa pine fires). An important note however is that these model results are lower limits that are applicable to the center of a young BB plume and do not include later dispersion, where non-BB sources of NO_x mixed with O_3 downwind generate NO_3 and lead to additional depletion of BB-NMOGs. This mixing effect is likely most significant in urban areas impacted by BB plumes. Urban sources of NO_x mixed with ambient background O_3 and elevated O_3 formed in aged plumes can contribute to additional oxidation and depletion of BB produced NMOGs.

4.2. NO_x

NO_x is effectively a precursor to two main atmospheric oxidants (O_3 and NO_3), and its chemistry is related to BrC as noted earlier. We note that for the majority of our sampling period, ($\geq$95% of the time), our NO values were below detection limits. Further, when we did briefly measure NO during smoke-impacted periods, the NO/NO_2 ratio was about ~0.23. Since we were not adjacent to combustion sources, our NO_x measurement is mostly a measurement of NO_2. NO_x/CO is usually about 1–2% in fresh forest fire plumes and after 2–3 hr NO_x is mainly converted to peroxyacetyl nitrate (PAN) and particle nitrate in roughly equal amounts with $\Delta PAN/\Delta CO$ observed as ~0.3% in aged wildfire smoke impacting Boise, ID (Akagi et al., 2011, 2012; Liu et al., 2016, 2017; McClure & Jaffe, 2018). Our 5-min data during smoke aged ~20 hr shows NO_2 as peaks that are ~20–30 ppb (about 10–15% of CO) and poorly correlated with CO confirming a mostly local source (Figures S1–S5). Some of the largest NO_x peaks occur after dark before midnight, and NO_2 peaks are dramatically anticorrelated with O_3, which is consistent with high NO_3 production rates (Figures S1–S5) We investigate the interaction with both wildfire and prescribed fire smoke in an analysis identical to the analysis done for O_3, whereby diurnal cycles of NO_x were plotted by computing hourly averages from 5-min NO_x data, for each hour of the day over the duration of the study. Figure 3 shows that there were no significant changes to the diurnal cycle of typical "clear-sky" concentrations of NO_x during either aged wildfire smoke-impacted periods or moderately fresh prescribed fire impacts. For the duration of the study, NO_x for both of the latter periods remained within the range of typical ambient concentrations, again suggesting our measured NO_x is likely the result of local emissions.

Plume dilution and rapid loss of NO_x as smoke is transported away from a fire suggest slowing of O_3 formation downwind. However, several studies show that urban sources of NO_x mixed with BB plumes can lead to an increase in O_3 (Jacob et al., 2010; Lee et al., 2009) and the highest O_3 formation rates in smoke plumes sampled by Akagi et al. (2013) occurred when a plume was mixed with urban emissions. Thus, our measurements of urban NO_x are likely critical to explaining some portion of the daytime O_3 enhancements discussed in the previous section.

4.3. NO_3 Production

P (NO_3) is the instantaneous formation rate of NO_3 through reaction of NO_2 and O_3 calculated via the following: P (NO_3) = $K_{NO3}[NO_2][O_3]$ (k = 3.2×10^{-17} cm^3 $molec^{-1}$ s^{-1} at 298 K; Burkholder et al., 2015). Reactions of NO_3 with many NMOGs are efficient and can lead to the production of organic nitrates and
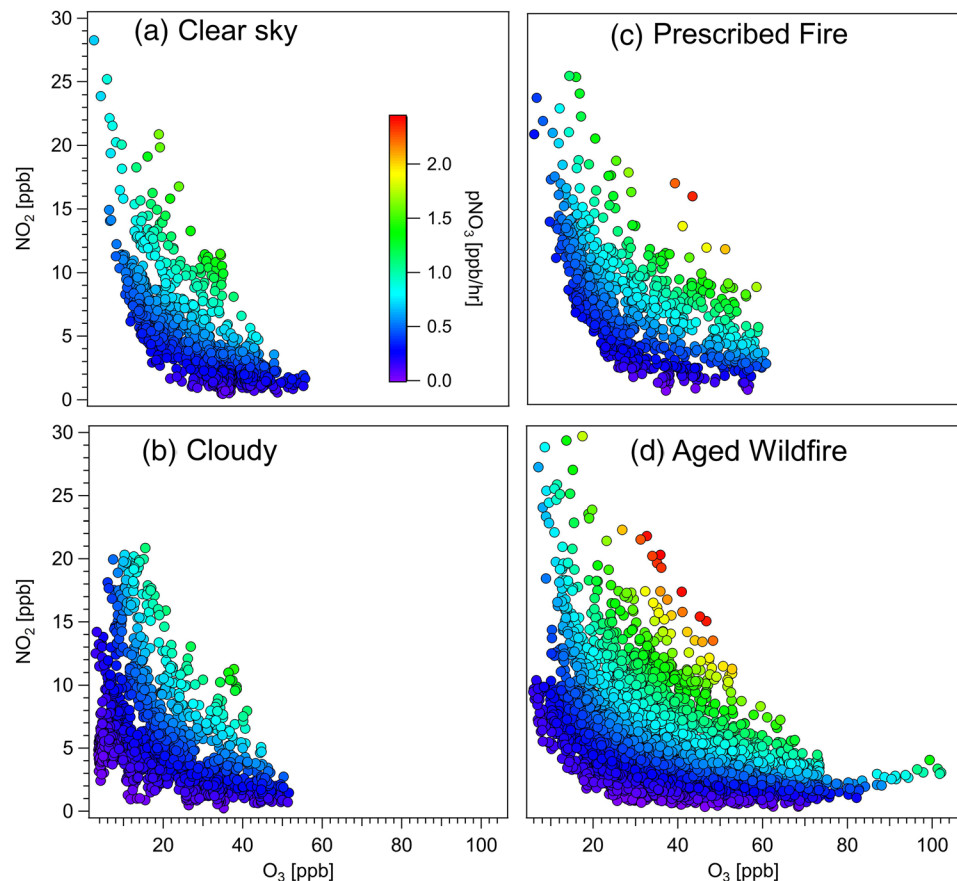
Figure 4. NO_2/O_3 plots colored by pNO_3. Panel (a) represents typical clear sky conditions, panel (b) represents cloudy and clean conditions, panel (c) represents prescribed-fire (3 hr old) smoke conditions, and panel (d) represents aged (up to several days) wildfire smoke-impacted conditions. Points with both low NO_2 and low O_3 during smoke-impacted periods arise from NO_2 titration of O_3 and not the inclusion of clear-sky data, which was filtered out as described in section 3.

SOA (Brown et al., 2012), altering nighttime oxidative budgets. Several studies show NO_3 leading to formation of secondary BrC aerosol, suggesting that nighttime oxidation may be a significant source of BB derived BrC, which has potential to affect next-day photochemistry (Iinuma et al., 2010; Laskin et al., 2015; Mohr et al., 2013; Palm et al., 2017). Using laboratory EFs measured at the Missoula Fire Sciences Lab in 2016 (Koss et al., 2018; Selimovic et al., 2018), Decker et al. (2019) modeled an NO_3 production rate (P (NO_3)) of 1 ppbv hr^{-1} in fresh plumes, and here we present complementary evidence of high P (NO_3) occurring in aged smoke. Although NO_3 is rapidly photolyzed during the day, we calculate P (NO_3) during night and day, because high NMOG concentrations and suppression of photolysis in thick smoke might make reactions of NO_3 competitive with photolysis. Figures S1–S5 show numerous P (NO_3) peaks above 1 ppb/hr and some above 2 ppb/hr. Figure 4 plots 5 min data of O_3 and NO_2 as a function of calculated P (NO_3). Although the highest instances of P (NO_3) were observed during wildfire smoke-impacted periods (2.44 ppbv hr^{-1}) (Figure 4d), on average, P (NO_3) was highest during prescribed fire impacts (Figure 4c).

The average P (NO_3) $\pm$ (1σ) for wildfire impacts was 0.57 ± 0.36 ppbv hr^{-1}, and the average for prescribed fire impacts was 0.66 ± 0.32 ppbv hr^{-1} although this particular comparison may depend less on smoke characteristics than some other comparisons. In both cases, P (NO_3) is higher than when compared with clear, smoke-free P (NO_3) (0.47 ± 0.26 ppbv hr^{-1}) and during cloudy periods (0.35 ± 0.25 ppbv hr^{-1}). In Figure 5, we investigate diurnal trends in P (NO_3) by calculating hourly averages from 5-min data of O_3 and NO_2 and then plotting them as a function of the hour of day. A weak trend shows that high P (NO_3)
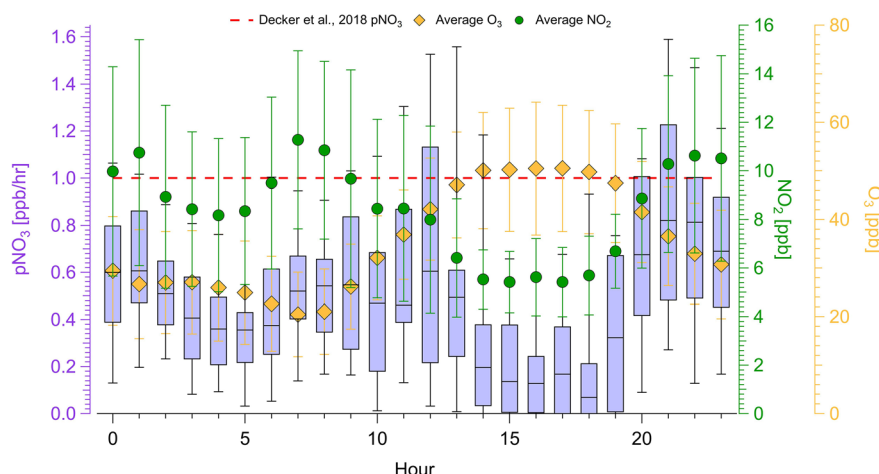
Figure 5. Hourly diurnal box and whisker plot of P (NO_3) plotted with hourly diurnal plots of O_3 and NO_2. Values were derived from hourly averages of 5-min wildfire smoke-impacted data. Error bars on O_3 and NO_2 represent 1σ.

is driven by large percentage increases in NO_2, which has implications for when/where NO_3 is formed. For example, at the plume source, where BB-NO_2 is abundant, NO_3 production is likely high, as shown in Decker et al. (2019). In addition, our data confirm that formation of NO_3 in smoke downwind of fires due to added NO_2 is also important and was most important after sunset. This is likely due to nonfire sources of NO_2 (urban) or, to a lesser degree, lightning and NO_2 from the thermal decomposition of fire-generated PAN mixing with enhanced levels of O_3 in aged plumes driving NO_3 production.

4.4. $\Delta BC/\Delta PM_{2.5}$, $\Delta BC/\Delta CO$, and $\Delta PM_{2.5}/\Delta CO$

We begin this section with a summary of the importance of the $\Delta BC/\Delta CO$, $\Delta BC/\Delta PM_{2.5}$, and $\Delta PM_{2.5}/\Delta CO$ ratios. Although BC is estimated to be the second strongest global climate warming agent, accurate measurements of ambient BC and BC EFs remain challenging, and aerosol absorption remains a large contributor to uncertainty in models (Bond et al., 2013; Li et al., 2019). CO emissions estimates are in reasonable agreement for western wildfires (Liu et al., 2017) and can be used to derive BC emissions estimates. For example, combining the measurements of these two inert tracers into a $\Delta BC/\Delta CO$ ratio can be used with CO emissions to update BC emissions estimates from wildfires, which could improve model input and further assist in validating current models. In addition, BC is only made by flaming combustion at the fire source, and although its production can vary with flame turbulence (Shaddix et al., 1994), the $\Delta BC/\Delta CO$ ratio can be used as a rough indicator of the fire flaming to smoldering ratio, as demonstrated in Selimovic et al. (2019). Turning to reactive species, a rough metric for the net effect of secondary formation and evaporation of OA and inorganic aerosol is provided by changes in the $\Delta PM/\Delta CO$ ratio as smoke ages. However, as referenced in section 1, there remains much ambiguity about the factors controlling the evolution of this ratio as smoke is transported downwind, and, in addition, few studies provide this ratio in heavily impacted surface locations, which is critical in assessing model predictions of surface AQ, especially as it relates to impacts on populated areas (Ahern et al., 2019; Bian et al., 2017; Lim et al., 2019; Morgan et al., 2020). BC/PM can also indicate PM evolution and roughly indicate climate impacts.

Table 1 reports our 2018 $\Delta BC/\Delta CO$, $\Delta PM_{2.5}/\Delta CO$, and $\Delta BC/\Delta PM_{2.5}$ mass ratios for aged wildfire smoke impacts and for the one fresher prescribed fire smoke impact. $\Delta BC/\Delta PM_{2.5}$ ratios were calculated by computing 1 hr averages of 5 min BC derived from PAX 870 absorption data and then plotted against 1 hr $PM_{2.5}$ data (Figure S7). In Figure S7 we plotted all the wildfire points together to show good overall correlation and illustrate one method of obtaining a time-weighted average. The individual $\Delta BC/\Delta PM_{2.5}$ ratios for the four 2018 wildfire-smoke events are 0.0183, 0.020, 0.0225, and 0.0242 (average 0.0213 ± 0.002 g g^{-1}) (Table S1). The variability is only about 10% of the mean, and the average computed this way is ~12% lower than plotting all points together. $\Delta BC/\Delta CO$ ratios were calculated as described in the methods section using integrated 5-min data to account for and maintain the high time resolution. $\Delta PM_{2.5}/\Delta CO$ was solved for using the two ratios calculated above.

Table 1
Study-Average Mass Enhancement Ratios (g g^{-1} Ratioed to CO) Compared to Ratios Reported in Other Studies

Study	Fire type[a]	Age (hr)	ΔBC/ΔCO	ΔPM$_{2.5}$/ΔCO	ΔBC/ΔPM$_{2.5}$
This work	WF	20 (10)	0.0026 (0.0007)	0.107 (0.0278)	0.0243 (0.0002)
	PF	~3	0.0026	0.165	0.0157 (0.0011)
Selimovic et al. (2019)[b,c]	WF	4–20	0.0014 (0.0006)	0.1263 (0.0015)	0.0107 (0.0003)
Garofalo et al. (2019)[d,e]	WF	0–6	—	0.201 (0.045)	—
McClure and Jaffe (2018)	WF	—	—	0.119 (0.01)	—
Liu et al. (2017)[b,d,e,f]	WF	0–2	0.0016 (0.0018)	0.2661 (0.1342)	0.0060 (0.0054)
Collier et al. (2016)[d,e]	WF	0–48	—	0.237 (0.082)	—
May et al. (2014)[b,c,d,g]	PF	0–0.5	0.006	0.11 (0.01)	0.048
Sahu et al. (2012)[b]	WF	—	0.0014	—	—

Note. Values in parenthesis represent 1σ. [a]WF stands for wildfire; PF stands for prescribed fire. [b]BC measurements at 1.0 micron cutoff. [c]BC values reported from 2017 have been adjusted up 13% to account for dryer and scrubber losses in the PAX instrumentation. [d]PM values reported are PM$_{1.0}$. [e]High-altitude samples. [f]Average of Rim Fire and Big Windy Complex. BC data were analyzed for Liu et al. (2017) but not reported. [g]Average of the Shaver and Turtle fires (prescribed burns in coniferous ecosystem in Sierra Nevada mountains).

We assess our results by comparing them in Table 1 to the previous 2017 measurements of ambient smoke in the Missoula valley (Selimovic et al., 2019) and to airborne measurements (Liu et al., 2017; May et al., 2014; Sahu et al., 2012). Our 2018 wildfire ΔBC/ΔCO ratio (0.0026 $\pm$ 0.0007) is roughly two times higher than in the 2017 wildfire smoke (0.0014 $\pm$ 0.0006) measured by Selimovic et al. (2019). While it is difficult to assess the exact reason for the 2017 to 2018 differences, a likely combination of several factors exists to potentially explain them. First, the wildfire smoke impacting Missoula in 2017 was from closer fires, which could enhance impacts of smoke more dominated by smoldering combustion and with lower BC/CO, as shown in Selimovic et al. (2019). Similarly, assuming BC and CO remain inert during transport, our higher ΔBC/ΔCO ratio in 2018 could be indicative of fire emissions more dominated by flaming combustion, which were lofted by convection and then transported to the Missoula valley. The PAX 870, which we use to derive our BC measurements, does not discriminate against any coating effects, so it is possible that our 2018 BC values are more inflated by lensing effects than in the younger 2017 smoke, and switching from a 1.0 to a 2.5 μm cyclone would add additional mass and could potentially lead to larger values in PAX 870 absorption. Even though BB-BC is nearly all submicron, other super micron components (microchar and dust) may absorb weakly and cause larger calculated values of BC (Clarke et al., 2004; Han et al., 2010). Although the mass in the 1.0–2.5 μm range is thought to be a small part of the total mass (Reid et al., 2005), the size range difference does affect data interpretation. In summary, despite the above caveats, it is significant that our ground-based, downwind 2-year average ΔBC/ΔCO (0.0020 $\pm$ 0.0007) is just 33% higher than the average of the airborne studies of western wildfires (0.0015 $\pm$ 0.0018) by Liu et al. (2017) and Sahu et al. (2012), as this is consistent with low bias of either platform toward flaming or smoldering combustion.

Selimovic et al. (2019) coupled the average annual CO emissions by wildfires for 2011–2015 (5,240 $\pm$ 2,240 Gg) from Liu et al. (2017) with their field average ΔBC/ΔCO (0.0014 $\pm$ 0.0002) to estimate that western U. S. wildfires emit 7.3 $\pm$ 3.3 Gg of BC a year. Using the same method described in that study, but now with 2 years of Missoula ΔBC/ΔCO data included in the field average (0.0018 $\pm$ 0.0006), we update that value to 9.4 $\pm$ 4.0 Gg of BC produced by wildfires per year. In addition, our ΔBC/ΔCO average across 2 years times the EF CO for wildfires measured in Liu et al. (2017) (89.3 $\pm$ 28.5) suggests an EF BC for wildfires of 0.18 $\pm$ 0.08 g kg^{-1}. Our ΔBC/ΔCO for the summer-time prescribed fire in coniferous fuels in this study (0.0026) is ~2.3 times less than the ΔBC/ΔCO ratio for fall (November) prescribed fire measurements in western U.S. montane fuels reported in May et al. (2014) (0.006), likely reflecting more smoldering consumption of duff and dead/down fuels in the summer prescribed fire.

Our surface ΔPM$_{2.5}$/ΔCO ratios for aged wildfire smoke across both years (0.1167 $\pm$ 0.0136) are consistently about half that of fresh wildfire smoke samples acquired at higher altitudes in airborne or mountain-top studies (0.2348 $\pm$ 0.0326) (Collier et al., 2016; Garofalo et al., 2019; Liu et al., 2017). Deposition is not a likely cause of our lower surface ΔPM$_{2.5}$/ΔCO since our surface ΔBC/ΔCO is not lower and we see evidence of supermicron aerosol in the plumes (section 4.6). In addition, our lower ΔPM$_{2.5}$/ΔCO ratios at the surface are consistent with some aircraft samples acquired at relatively lower elevations and latitudes and likely

warmer temperatures (Capes et al., 2008; Forrister et al., 2015). Other ground-based observations of wildfire smoke have seen $PM_{2.5}$/CO ratios similar to our Missoula ratio (0.119 ± 0.01; McClure & Jaffe, 2018). This reinforces the observation from Selimovic et al. (2019) that on timescales up to ~1–2 days, aging and/or higher ambient temperatures at the surface may lead to substantial net OA evaporation. This decrease with age may not occur at high altitude but significantly reduce downwind surface PM impacts. Our $\Delta PM_{2.5}/\Delta CO$ value (0.165) for the fresher prescribed fire smoke (~3 hr old) is higher than both our 2017 and 2018 values for aged wildfire smoke but still significantly lower than the airborne wildfire average from Liu et al. (2017). Our summer prescribed fire $\Delta PM_{2.5}/\Delta CO$ ratio is higher than our wildfire ratio but has a similar $\Delta BC/\Delta CO$ ratio (at least for 2018). One potential simple explanation is distance, in that the summer prescribed fire was closer to the Missoula valley than the wildfires impacting the valley during that same year and thus experienced less dilution-driven evaporation. Additionally, lower surface temperatures (8–29°C) during the time of the prescribed fire impact, in comparison to temperatures during some of the wildfire impacts, may have been less conducive to PM evaporation (Li & Shiraiwa, 2019). The ~15% higher $\Delta PM_{2.5}/\Delta CO$ ratio for 2017 wildfire smoke in Missoula may reflect younger average smoke age (Selimovic et al., 2019). Our summer prescribed fire $\Delta PM_{2.5}/\Delta CO$ ratio is 50% higher than the ratio reported for fresh smoke from the fall prescribed fires in western montane fuels in May et al. (2014) (0.11), but May et al. (2015) also note that their $\Delta PM_{1.0}/\Delta CO$ decreased by about a factor of 2 after several hours of aging on at least one prescribed fire. Fuel and measurement differences (additional mass in the 1.0–2.5 μm range) mentioned earlier could also both potentially account for some of the higher PM/CO produced by the summer prescribed fire.

We stress that there is now more than 1,000 hr of ground-based data from Missoula, suggesting that a typical $PM_{2.5}$/CO value for aged wildfire smoke at the surface is about half the value in fresh to moderately aged well-lofted wildfire plumes (Collier et al., 2016; Garofalo et al., 2019; Liu et al., 2017). One airborne wildfire study by Forrister et al. (2015) at lower latitudes and sampling elevations than the other airborne studies is consistent with the downwind net evaporation we apparently observe in Missoula. We also stress that, despite the evidence for PM evaporation during aging, there are strong data discussed next, supporting the idea that wildfires produce more PM than spring or fall prescribed fires on a per fuel burned or per area burned basis. Liu et al. (2017) reported that EFs for $PM_{1.0}$ ($gPM_{1.0}$/kg fuel burned) are almost four times higher in wildfires (27.1 ± 6.1) than spring and fall prescribed fires (7.3 ± 4.2; May et al., 2014). Our 2 year average $\Delta PM_{2.5}/\Delta CO$ ratio in aged wildfire smoke (~0.117) is ~1.7 times higher than implied for aged, fall western montane prescribed fire smoke (~0.07) based on May et al. (2014, 2015), suggesting that a remnant of the difference in initial PM emissions can survive aging. Fuel consumption in spring/fall prescribed fires at the national level is typically 7.2 ± 2.7 Mg ha^{-1} (Yokelson et al., 1999, 2013) as opposed to 34.6 ± 9.9 Mg ha^{-1} on wildfires (Campbell et al., 2007; Santín et al., 2015). Combining the emissions and fuel consumption differences implies that wildfires emit 18 ± 14 times more PM per area burned. Although prescribed fires cannot simply replace all wildfires (Schoennagel et al., 2017; Turner et al., 2019), their potential to reduce the level of wildfire impacts deserves more attention. In addition, incorporating higher wildfire initial emissions and temperature-dependent, postemission OA evaporation may improve models of wildfire smoke impacts (Nergui et al., 2017).

Our study average $\Delta BC/\Delta PM_{2.5}$ ratio for wildfire smoke in 2018 is roughly double our $\Delta BC/\Delta PM_{2.5}$ ratio for 2017 wildfire smoke (Selimovic et al., 2019) and approximately four times higher than the aircraft average $\Delta BC/\Delta PM_{1.0}$ for 2013 wildfires (Liu et al., 2017; Selimovic et al., 2019). Likely reasons for the higher ratio in 2018 include the possible reasons for a higher BC/CO ratio in 2018 mentioned above: for example, increased lensing in more aged smoke, transport of more flaming smoke, and (less likely) including other absorbers with the $PM_{2.5}$ cutoff. In addition, $BC/PM_{2.5}$ could be higher in 2018 aged wildfire smoke because of more time (on average) for PM evaporation. OA is the main component of wildfire PM (Liu et al., 2017; Schlosser et al., 2017), so the $\Delta BC/\Delta PM$ ratio should be similar to the $\Delta BC/\Delta OA$ ratio, which suggests a "low" MAC in the UV for the wildfire OA (Saleh et al., 2014; section 4.6). Our low $\Delta BC/\Delta PM_{2.5}$ ratios across both years (~1–2%), along with high SSA (section 4.6), further confirm that wildfire aerosol is overwhelmingly organic and strongly cooling. Our summer prescribed fire $\Delta BC/\Delta PM_{2.5}$ is approximately three times lower than the ratio reported for fall prescribed fires in similar fuels in May et al. (2014), which is likely (as noted above) because drier summer burning conditions enable consumption of fuels (e.g., dead/down and duff) that tend to burn by smoldering but are too wet to burn as completely in spring/fall. While we

Table 2
Study-Average AAE and %BrC Contribution to Absorption at 401 nm Compared to Other Studies

Ratios	Fire type	This work	Selimovic et al. (2019)	Selimovic et al. (2018)[a]
AAE	WF	1.71 (0.04)	1.96 (0.38)	3.31
	PF	2.49 (0.04)	—	
%BrC	WF	46.55 (0.51)	50.72 (12.78)	78
	PF	70.79 (0.42)	—	—

Note. Values in parentheses represent 1σ.
[a]Lab fires, calculated from the average of wildfire MCE reported in Forrister et al. (2015).   [b]WF stands for wildfire; PF stands for prescribed fire. Wildfire smoke was more aged (up to several days) than prescribed fire smoke (~3 hr).

indicate above that wildfires are likely smokier than spring/fall prescribed fires, which has poor implications for AQ, they also appear to have less positive climate forcing. In any case, we reiterate that differences in smoke production and chemistry between wildfires and prescribed fires warrants further research, as more definite conclusions can reinforce land management implications.

4.5. UV Absorption by BrC and AAE

The AAE is an important aerosol optical parameter used for characterization and apportionment studies. Further, the AAE can be used to separate BrC from BC absorption (Liu et al., 2018), and higher AAEs are correlated with absorption that is more dominated by BrC (Pokhrel et al., 2016, 2017; Selimovic et al., 2018, 2019). A lab study with wildfire fuels found that BrC accounted for ~86% of absorption by particles in the UV (401 nm) on average in fresh smoke (AAE of 3.50), which has implications for UV-driven photochemical reactions of O_3 and the lifetimes of, for example, NO_x and HONO (Selimovic et al., 2019). Satellite AAE retrievals and one airborne study indicate that BrC can have a strong impact in fresh wildfire plumes (AAE 2.8–3.75) and significant, persistent impacts in downwind regional haze/plumes (Forrister et al., 2015; Hammer et al., 2016; Jethva & Torres, 2011). There is variability in BrC attribution methods across studies (Forrister et al., 2015; Pokhrel et al., 2017), but despite this, BrC absorption would decrease the climate cooling calculated for purely scattering OA depending on its MAC, lifetime, and the amount emitted (Feng et al., 2013; Forrister et al., 2015). Furthermore, sources of BrC not directly emitted from BB, including the photo-oxidation of NMOGs need to be considered. However, these complex processes produce BrC with optical properties and lifetime that are not yet comprehensively evaluated. Mixing state, combustion conditions, chemical transformation, and photochemical aging are all factors that can influence the absorption of secondary BrC (Ervens et al., 2011; Fleming et al., 2020; Graber & Rudich, 2006; Laskin et al., 2015; Tomaz et al., 2018; Wang et al., 2014, 2017).

In Table 2 we present 2 years of in situ smoke/haze data from Missoula showing persistent widespread regional impacts of BrC and the associated AAE values. Smoke age is a key factor. In 2017 the episode with the highest AAE (2.88, 77% BrC absorption at 401 nm) was due to smoke from a wildfire just ~2–4 hr upwind and the 2017 average AAE (for smoke 2–48 hr old) was 1.96 ± 0.38 (51% BrC absorption at 401 nm). The 2018 wildfire smoke was more aged on average (no nearby wildfires) and had a lower study-average AAE of 1.71 ± 0.04 (47% BrC absorption at 401 nm), but the one relatively fresh prescribed fire smoke episode in 2018 had a higher than average AAE of 2.49 (71% BrC absorption at 401 nm).

Remarkably, despite the large range in episode smoke ages across both years, BrC accounted for roughly 50% of the UV absorption at 401 nm on average both years. The small ~4% difference in % BrC absorption at 401 nm year to year likely indicates that the decrease after emission in net BrC slows significantly after a few hours similar to the observations in the Rim Fire plume (Forrister et al., 2015). In any case obtaining the same average value for moderately aged smoke 2 years in a row suggests our regional smoke AAE value (~1.7–1.9) is a useful target for model validation, which would be hard to demonstrate in lab studies or airborne studies of a single plume.

It is interesting to speculate about the impact of combustion conditions and nighttime effects on multiday aging of BrC. Selimovic et al. (2018) showed that higher AAE in the initial emissions is associated with more smoldering combustion. Relatively more smoldering as demonstrated by the lower ΔBC/ΔCO ratio in 2017 could have contributed to the higher AAE in 2017 (along with differences in smoke age). In addition, wildfires can produce much of their emissions at times of day shortly before or after photobleaching would stop (Saide et al., 2015), and wildfires can have a higher smoldering to flaming ratio at night than during the day (Benedict et al., 2017), which would likely enhance emissions of both primary BrC (Selimovic et al., 2018) and BrC precursors. Precursors include monoterpenes, furans, and so forth, which can react with the major nighttime oxidant, NO_3 to form UV-absorbing organic nitrates. Estimates using current NMOG data strongly suggest that a substantial nighttime secondary BrC source could exist (Gilman et al., 2015; Hatch et al., 2017; Stockwell et al., 2015). Converting even a small fraction of coemitted NMOGs that are known to react quickly with NO_3 could yield substantial amounts of BrC during dark hours, and oxidation of
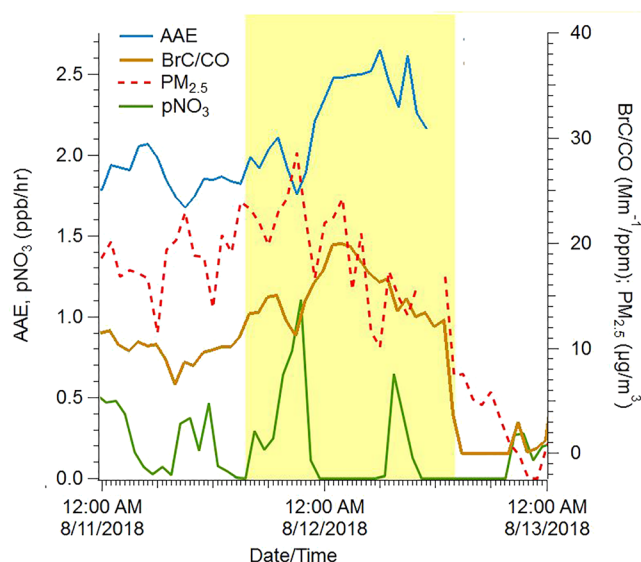
Figure 6. A likely example of nighttime, secondary BrC formation. Shortly before midnight a spike in P (NO$_3$) occurs, followed by increases in AAE and BrC/CO as PM$_{2.5}$ decreases, which rules out an influx of fresh smoke. These changes are consistent with increasing BrC content of the aerosol driven by reactions of NO$_3$ with NMOG.

NMOGs by O$_3$ could also be important, as mentioned earlier in sections 1 and 4.1. Our 5-min data in Figure S1 or our 1-hr data in Figure 6 show a potential example of this. Shortly before 12 a.m. on 12 August, there is a spike in NO$_3$ production followed by a prominent increase in AAE (from ~1.6 to ~3.0) that lasts until sunrise. The increase in AAE is likely not due to arrival of fresher, usually more concentrated, smoke, which we also commonly see, since hourly PM$_{2.5}$ is simultaneously decreasing.

In Figure 7, we show the diurnal cycle of % absorption by BrC at 401 nm, with nighttime production of NO$_3$. The % absorption by BrC at 401 nm is slightly enhanced at night (11%) and loosely follows the NO$_3$ production (enhanced by 29% at night) consistent with a role for the effects discussed above. However, with the data available, we cannot completely separate the potential effects of nighttime NO$_3$ reactions, enhanced smoldering emissions, or transport/mixing. Nonetheless, the presence of NO$_3$ as a major nighttime oxidant in the formation of BrC should be considered, as our high NO$_3$ production rates in an earlier section (section 4.3) show.

4.6. SSA, MAC, and MSC

Table 3 lists our 2018 study average SSAs, MACs, and MSCs. MACs and MSCs can be coupled with PM$_{2.5}$ data to describe the optical properties of aerosol on a per mass basis. Our MAC and MSC values were obtained by plotting 1 hr averages of $B_{scat}401$, $B_{abs}401$, and $B_{scat}870$, $B_{abs}870$ versus the 1 hr PM$_{2.5}$ values in order to calculate an MSC(401), MAC(401), MSC(870), and MAC(870) (Figures S8–S11). In Selimovic et al. (2019), we produced MAC and MSC values by comparing our scattering and absorption measurements measured at a 1.0 μm cutoff to PM$_{2.5}$ data that was available. These values were lower limits and are not directly comparable to the ones obtained in this study, where the range for both optical and mass measurements goes up to 2.5 μm. Nonetheless, it is useful to list the results from both studies as a range of values, since 1.0 μm cutoffs are common in field campaigns, but PM$_{2.5}$ still remains the default measurement in regional networks. We again reiterate that going to a PM$_{2.5}$ cutoff may have added ash, microchar and aerosol that is noncombustion generated, such as dust or primary biological aerosol particles, all of which can be physically entrained in wildfire plumes (Formenti et al., 2003; Gaudichet et al., 1995;
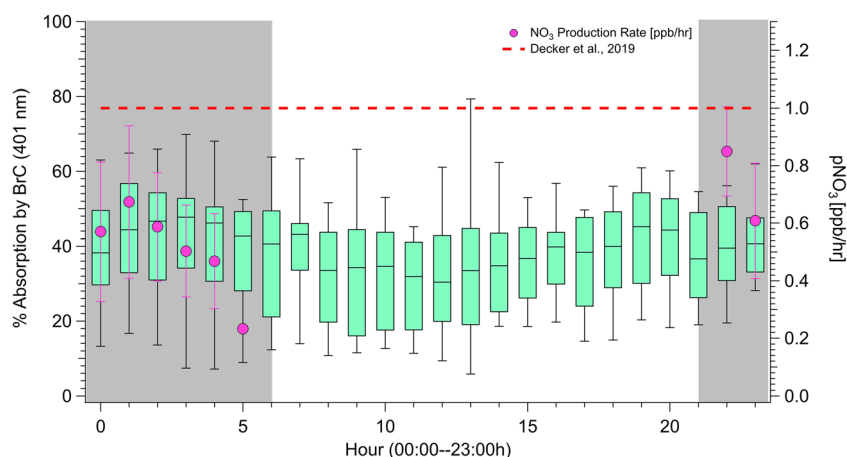

Figure 7. Hourly diurnal box and whisker plot of % absorption by BrC calculated from hourly averages of wildfire smoke-impacted 5-min data compared to the nighttime (shaded area) hourly average P (NO$_3$). Error bars on P (NO$_3$) represent 1σ.

Table 3
Study-Average MAC and MSC Compared to Other Works

Parameter	λ (nm)	This work[a] (WF)	This work[a] (PF)	Selimovic et al. (2019)[b,c]
SSA	401	0.95 (<0.01)	0.95	0.93 (0.01)
	870	0.95 (<0.01)	0.94	0.94 (0.02)
MAC	401	0.43 (0.01)	0.46 (0.03)	0.26 (0.01)
	401 (BrC)	0.18	0.29	0.16
	870	0.12 (<0.01)	0.07 (0.01)	0.05 (<0.01)
MSC	401	7.37 (0.06)	5.88 (0.39)	3.65 (0.07)
	530	4.70	3.25	2.41
	870	2.12 (0.02)	1.13 (0.09)	1.14 (0.02)

Note. Units are in $m^2\ g^{-1}$. Values in parentheses represent 1σ.
[a]In this work MAC and MSC values are $PM_{2.5}$ absorption and scattering values divided by $PM_{2.5}$ mass, and values between 401 and 870 nm are obtained from power law fits. [b]In this work MAC and MSC values are $PM_{1.0}$ absorption and scattering values divided by $PM_{2.5}$ mass, and values between 401 and 870 nm are obtained from power law fits. [c]MAC and MSC values have been adjusted 13% to account for dryer loss in the PAX instrumentation. SSA is unaffected by this loss.

Hungershoefer et al., 2008; Mardi et al., 2018; Maudlin et al., 2015; Schlosser et al., 2017; Shingler et al., 2016).

Several things stand out comparing 2017 and 2018 data in Table 3. The SSA(401) is lower in 2017 (0.93) than 2018 (0.95), but SSA(870) is similar both years, consistent with the 2017 smoke being fresher and with higher BrC content. MAC(401) and MAC(870) almost doubled from 2017 to 2018. Since our $\Delta BC/\Delta PM_{2.5}$ also approximately doubled, this makes sense and is not inconsistent with the work of Saleh et al. (2014), who found that the MAC for OA increased with BC/OA (wildfire PM is mostly OA). A contribution to UV absorption from the increased cutoff and thereby sampling more entrained microchar or dust (Han et al., 2015; Russell et al., 2010) could also play a role. The latter is supported by the ~25% increase in calculated MSC(530). Although the particles in the 1.0–2.5 μm range contribute perhaps 20% of the total particle mass in BB emissions (Reid et al., 2005), they contributed significantly to both the total absorption and scattering in 2017–2018 smoke but did not strongly affect the SSA.

The SSA is frequently used to calculate aerosol absorption and scattering in models and satellite retrievals. Uncertainty in the SSA is one of the main sources of uncertainty in estimating the radiative effect of aerosols (Jiang & Feingold, 2006; McComiskey et al., 2008), and assuming constant values of SSA throughout the year may sometimes be inaccurate, as shown by Selimovic et al. (2019) in 2017 in Missoula, where the SSA at 870 nm in Missoula increased over a month, and Eck et al. (2013), where the SSA at 530 nm in Southern Africa increased by 0.07 between July and October. These increases are consistent with an increase in the smoldering/flaming ratio as regional fuels dry (Akagi et al., 2011; Liu et al., 2014; Pokhrel et al., 2016; Selimovic et al., 2019). Our 2018 study average wildfire SSA at 401 nm is slightly higher than the 2017 study average SSA observed in Selimovic et al. (2019), but our 2018 SSA at 870 nm falls within the observed variability for SSA at 870 nm in 2017. Our values at both wavelengths are higher than a typical surface SSA of the Earth (~0.9; Praveen et al., 2012), which suggests that overall, the wildfire PM measured in this study would contribute to regional cooling (Kolusu et al., 2015; Thornhill et al., 2018). However, Figure 8 shows we do not find an increase in either the SSA at 870 nm or the SSA at 401 nm over the duration of our 2018 sampling period. SSA has been shown to increase as smoke ages (Haywood et al., 2003; Liu et al., 2014; Yokelson et al., 2009), and the additional aging in the 2018 smoke may have obscured any trend based on flaming or smoldering sources, as we received little impact from local sources in 2018, unlike in 2017 (Selimovic et al., 2019).

5. Conclusions

In this study, we measured smoke properties during the summer of 2018 in Missoula, MT, a western urban center that was downwind of numerous wildfires and one prescribed fire. We sampled over 500 hr of smoke impacts characterizing CO, aerosol optical properties, effects of wildfire and prescribed fire smoke on O_3 and NO_3 production and explored how inert tracers and evolving ratios inform understanding of smoke production and evolution. By comparing and combining with our measurements of less aged smoke in Missoula from 2017, we analyze data for over 1,000 hr of ambient smoke from western wildfires primarily in coniferous forests. Our low 2 year $\Delta BC/\Delta PM$ average (0.0175 ± 0.0094) confirms the overwhelmingly organic and thus strongly cooling nature of wildfire
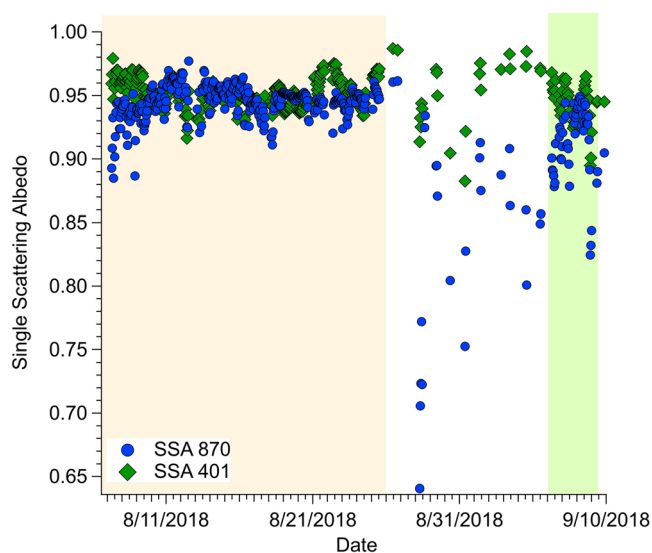

Figure 8. Plot of single scattering albedo at 401 and 870 nm versus the entirety of the sampling duration, calculated for each hour. Sections shaded in pink represent wildfire smoke-impacted periods. Sections shaded in green represent prescribed fire smoke-impacted periods. Unshaded areas represent anthropogenic impacts.

smoke and is in line with observations from other field studies. Our 2018 $\Delta BC/\Delta CO$ ratio (0.0026 ± 0.0007) is almost double the ratio measured in 2017 in Missoula and suggests a greater influence from lofted smoke produced by flaming combustion, but the average of our $\Delta BC/\Delta CO$ ratio across 2 years (0.0020 ± 0.0007) is close to airborne field observations of wildfire smoke, implying low sampling bias between platforms. Conversely, $\Delta PM/\Delta CO$ measured at our surface site across both years was consistently ~50% lower than field studies conducted at higher elevations suggesting that OA evaporation at higher temperatures near the surface may reduce wildfire PM AQ impacts.

On average, O_3 was enhanced when aged wildfire smoke was present by ~15% (6 ppb) relative to typical clear-sky levels, with the largest percentage enhancements occurring after sunset and before midnight. The larger O_3 increase after dark likely implies widespread, regionally enhanced O_3 production upwind, but the arrival of thicker smoke just before dark during the prescribed fire impact may have suppressed morning O_3 formation. There appeared to be no smoke impacts on the diurnal cycle of NO_x, suggesting that for the duration of the study, NO_x was likely the result of local emissions. However, NO_3 production rates were significant and slightly elevated relative to background conditions when both wildfire and prescribed fire smoke were present.

On at least one occasion, a nighttime increase in AAE followed, and was likely due to, a spike in P (NO_3) promoting reactions of NO_3 with NMOG. On average, the contribution to absorption at 401 nm by BrC was slightly enhanced at night and loosely followed NO_3 production, but this warrants more study. Despite the large range in episodic smoke ages across both years, BrC accounted for roughly 50% of the UV absorption at 401 on average, signifying wide-spread persistence of BrC even as smoke ages and is transported downwind. Obtaining similar AAE values for moderately aged smoke 2 years in a row implies that our regional smoke AAE value (1.7–2.0) is a useful target for model validation. The SSA at both wavelengths remained fairly constant over the course of the wildfire sampling period in 2018 but was higher than the SSA at both wavelengths for anthropogenic aerosol.

Conflict of Interest

The authors declare that they have no competing interests.

Data Availability Statement

Time series of data used in this paper can be found online (at https://osf.io/dkjt7/).

References

Abatzoglou, J. T., & Williams, A. P. (2016). Impact of anthropogenic climate change on wildfire across western US forests. *Proceedings of the National Academy of Sciences of the United States of America*, *113*(42), 11,770–11,775. https://doi.org/10.1073/pnas.1607171113

Ahern, A. T., Robinson, E. S., Tkacik, D. S., Saleh, R., Hatch, L. E., Barsanti, K. C., et al. (2019). Production of secondary organic aerosol during aging of biomass-burning smoke from fresh fuels and its relationship to VOC precursors. *Journal of Geophysical Research: Atmospheres*, *124*, 3583–3606. https://doi.org/10.1029/2018JD029068

Akagi, S. K., Craven, J. S., Taylor, J. W., McMeeking, G. R., Yokelson, R. J., Burling, I. R., et al. (2012). Evolution of trace gases and particles emitted by a chaparral fire in California. *Atmospheric Chemistry and Physics*, *12*(3), 1397–1421. https://doi.org/10.5194/acp-12-1397-2012

Akagi, S. K., Yokelson, R. J., Burling, I. R., Meinardi, S., Simpson, I., Blake, D. R., et al. (2013). Measurements of reactive trace gases and variable O_3 formation rates in some South Carolina biomass burning plumes. *Atmospheric Chemistry and Physics*, *13*(3), 1141–1165. https://doi.org/10.5194/acp-13-1141-2013

Akagi, S. K., Yokelson, R. J., Wiedinmyer, C., Alvarado, M. J., Reid, J. S., Karl, T., et al. (2011). Emission factors for open and domestic biomass burning for use in atmospheric models. *Atmospheric Chemistry and Physics*, *11*(9), 4039–4072. https://doi.org/10.5194/acp-11-4039-2011

Ambrose, J. L., Reidmiller, D. R., & Jaffe, D. A. (2011). Causes of high O3 in the lower free troposphere over the Pacific Northwest as observed at the Mt. Bachelor Observatory. *Atmospheric Environment*, *45*, 5302–5315. https://doi.org/10.1016/j.atmosenv.2011.06.056

Baylon, P., Jaffe, D. A., Hall, S. R., Ullmann, K., Alvarado, M. J., & Lefer, B. L. (2018). Impact of biomass burning plumes on photolysis rates and ozone formation at the mount bachelor observatory. *Journal of Geophysical Research: Atmospheres*, *123*, 2272–2284. https://doi.org/10.1002/2017JD027341

Benedict, K. B., Prenni, A. J., Carrico, C. M., Sullivan, A. P., Schichtel, B. A., & Collett, J. L. Jr. (2017). Enhanced concentrations of reactive nitrogen species in wildfire smoke. *Atmospheric Environment*, *148*, 8–15. https://doi.org/10.1016/j.atmosenv.2016.10.030

Bertschi, I. T., Yokelson, R. J., Goode, J. G., Ward, D. E., Babbitt, R. E., Susott, R. A., & Hao, W. M. (2003). Trace gas and particle emissions from fires in large diameter and belowground biomass fuels. *Journal of Geophysical Research*, *108*(D13), 8472. https://doi.org/10.1029/2002JD002100

Bian, Q., Jathar, S. H., Kodros, J. K., Barsanti, K. C., Hatch, L. E., May, A. A., et al. (2017). Secondary organic aerosol formation in biomass-burning plumes: Theoretical analysis of lab studies and ambient plumes. *Atmospheric Chemistry and Physics*, *17*(8), 5459–5475. https://doi.org/10.5194/acp-17-5459-2017

Birks, J. W., Andersen, P. C., Williford, C. J., Turnipseed, A. A., Strunk, S. E., Ennis, C. A., & Mattson, E. (2018). Folded tubular photometer for atmospheric measurements of NO$_2$ and NO. *Atmospheric Measurement Techniques*, *11*, 2821–2835. https://doi.org/10.5194/amt-11-2821-2018

Birks, J. W., Williford, C. J., Andersen, P. C., Turnipseed, A. A., Strunk, S., & Ennis, C. A. (2018). Portable ozone calibration source independent of changes in temperature, pressure and humidity for research and regulatory applications. *Atmospheric Measurement Techniques*, *11*, 4797–4807. https://doi.org/10.5194/amt-11-4797-2018

Bond, T. C., & Bergstrom, R. (2006). Light absorption by carbonaceous particles: An investigative review. *Aerosol science and technology*, *40*, 27–67. https://doi.org/10.1080/02786820500421521

Bond, T. C., Doherty, S. J., Fahey, D. W., Forster, P. M., Berntsen, T., DeAngelo, B. J., et al. (2013). Bounding the role of black carbon in the climate system: A scientific assessment. *Journal of Geophysical Research: Atmospheres*, *118*, 5380–5552. https://doi.org/10.1002/jgrd.50171

Bond, T. C., Streets, D. G., Yarber, K. F., Nelson, S. M., Woo, J.-H., Klimont, Z., & Z. (2004). A technology-based global inventory of black and organic carbon emissions from combustion. *Journal of Geophysical Research*, *109*, D14203. https://doi.org/10.1029/2003JD003697

Bowman, K. W., Liu, J., Bloom, A. A., Parazoo, N. C., Lee, M., Jiang, Z., & Menemenlis, D. (2017). Global and Brazilian carbon reponse to El Nino Modoki 2011—2010. *Earth and Space Science*, *4*, 637–660. https://doi.org/10.1002/2016EA000204

Braun, R. A., Dadashazar, H., MacDonald, A. B., Aldhaif, A. M., Maudlin, L. C., Crosbie, E., et al. (2017). Impact of wildfire emissions on chloride and bromide depletion in marine aerosol particles. *Environmental Science & Technology*, *51*(16), 9013–9021. https://doi.org/10.1021/acs.est.7b02039

Brey, S. J., & Fischer, E. V. (2016). Smoke in the City: How often and where does smoke impact summertime ozone in the United States? *Environmental Science & Technology*, *50*, 1288–1294. https://doi.org/10.1021/acs.est.5b05218

Brown, S. S., Dubé, W. P., Bahreini, R., Middlebrook, A. M., Brock, C. A., Warneke, C., et al. (2013). Biogenic VOC oxidation and organic aerosol formation in an urban nocturnal boundary layer: Aircraft vertical profiles in Houston. *TX. Atmospheric Chemistry & Physics*, *13*, 11,317–11,337. https://doi.org/10.5194/acp-13-11317-2013

Brown, S. S., Dubé, W. P., Karamchandani, P., Yarwood, G., Peischl, J., Ryerson, T. B., et al. (2012). The effects of NOx control and plume mixing on nighttime chemical processing of plumes from coal-fired power plants. *Journal of Geophysical Research*, *117*, D07304. https://doi.org/10.1029/2011JD016954

Burkholder, J. B., Sander, S. P., Abbatt, J., Barker, J. R., Huie, R. E., Kolb, C. E., & Kurylo, M. J. (2015). *Chemical kinetics and photochemical data for use in atmospheric studies, evaluation No. 18*. Pasadena, CA: JPL Publication, Jet Propulsion Laboratory. http://jpldataeval.jpl.nasa.gov

Burling, I. R., Yokelson, R. J., Akagi, S. K., Urbanski, S. P., Wold, C. E., Griffith, D. W. T., et al. (2011). Airborne and ground-based measurements of the trace gases and particles emitted by prescribed fires in the United States. *Atmospheric Chemistry and Physics*, *11*, 12,197–12,216. https://doi.org/10.5194/acp-11-12197-2011

Campbell, J., Donato, D., Azuma, D., & Law, B. (2007). Pyrogenic carbon emission from a large wildfire in Oregon, United States. *Journal of Geophysical Research*, *112*, G04014. https://doi.org/10.1029/2007JG000451

Capes, G., Johnson, B., McFiggans, G., Williams, P. I., Haywood, J., & Coe, H. (2008). Aging of biomass burning aerosols over West Africa: Aircraft measurements of chemical composition, microphysical properties, and emission ratios. *Journal of Geophysical Research*, *113*, D00C15. https://doi.org/10.1029/2008JD009845

Chen, J., Li, C., Ristovski, Z., Milic, A., Gu, Y., Islam, M. S., et al. (2017). A review of biomass burning: Emissions and impacts on air quality, health, and climate in China. *Science of the Total Environment*, *579*, 1000–1034. https://doi.org/10.1016/j.scitotenv.2016.11.025

Clarke, A. D., Shinozuka, Y., Kapustin, V. N., Howell, S., Huebert, B., Doherty, S., et al. (2004). Size distributions and mixtures of dust and black carbon aerosol in Asian outflow: Physiochemistry and optical properties. *Journal of Geophysical Research*, *109*, D15S09. https://doi.org/10.1029/2003jd004378

Collier, S., Zhou, S., Onasch, T. B., Jaffe, D. A., Kleinman, L., Sedlacek, A. J. I. I. I., et al. (2016). Regional influence of aerosol emissions from wildfires driven by combustion efficiency: Insights from the BBOP campaign. *Environmental Science & Technology*, *50*(16), 8513–8522. https://doi.org/10.1021/acs.est.6b01617

Crutzen, P. J., & Andreae, M. O. (1990). Biomass burning in the tropics: Impact on atmospheric chemistry and biogeochemical cycles. *Science*, *250*, 1669–1678. https://doi.org/10.1126/science.250.4988.1669

Cubison, M. J., Ortega, A. M., Hayes, P. L., Farmer, D. K., Day, D., Lechner, M. J., et al. (2011). Effects of aging on organic aerosol from open biomass burning smoke in aircraft and laboratory studies. *Atmospheric Chemistry and Physics*, *11*, 12,049–12,064. https://doi.org/10.5194/acp-11-12049-2011

Decker, Z. C. J., Zarzana, K. J., Coggon, M., Min, K. E., Pollack, I., Ryerson, T. B., et al. (2019). Nighttime chemical transformation in biomass burning plumes: A box model analysis initialized with aircraft observations. *Environmental Science & Technology*, *53*(5), 2529–2538. https://doi.org/10.1021/acs.est.8b05359

Doerr, S. H., & Santín, C. (2016). Global trends in wildfire and its impacts: Perceptions versus realities in a changing world. *Philosophical Transactions of the Royal Society B: Biological Sciences*, *371*(1696), 20150345. https://doi.org/10.1098/rstb.2015.0345

Draxler, R. R. (1999). *HYSPLIT4 user's guide. NOAA Tech. Memo. ERL ARL-230*. Silver Spring, MD: NOAA Air Resources Laboratory.

Draxler, R. R., & Hess, G. D. (1997). *Description of the HYSPLIT_4 modeling system. NOAA Tech. Memo. ERL ARL-224*. (p. 24). Silver Spring, MD: NOAA Air Resources Laboratory.

Draxler, R. R., & Hess, G. D. (1998). An overview of the HYSPLIT_4 modeling system of trajectories, dispersion, and deposition. *Australian meteorological magazine*, *47*, 295–308.

Eck, T. F., Holben, B. N., Reid, J. S., Mukelabai, M. M., Piketh, S. J., Torres, O., et al. (2013). A seasonal trend of single scattering albedo in southern African biomass-burning particles: Implications for satellite products and estimates of emissions for the world's largest biomass-burning source. *Journal of Geophysical Research: Atmospheres*, *118*, 6414–6432. https://doi.org/10.1002/jgrd.50500

Ervens, B., Turpin, B. J., & Weber, R. J. (2011). Secondary organic aerosol formation in cloud droplets and aqueous particles (aqSOA): A review of laboratory, field and model studies. *Atmospheric Chemistry and Physics*, *11*(21), 11,069–11,102. https://doi.org/10.5194/acp-11-11069-2011

Feng, Y., Ramanathan, V., & Kotamarthi, V. R. (2013). Brown carbon: A significant atmospheric absorber of solar radiation? *Atmospheric Chemistry and Physics*, *13*, 8607–8621. https://doi.org/10.5194/acp-13-8607-2013

Fleming, L. T., Lin, P., Roberts, J. M., Selimovic, V., Yokelson, R., Laskin, J., et al. (2020). Molecular composition and photochemical lifetimes of brown carbon chromophores in biomass burning organic aerosol. *Atmospheric Chemistry and Physics*, *20*(2), 1105–1129. https://doi.org/10.5194/acp-20-1105-2020

Ferguson, S. A., Collins, R. L., Ruthford, J., & Fukuda, M. (2003). Vertical distribution of nighttime smoke following a wildland biomass fire in boreal Alaska. *Journal of Geophysical Research*, *108*(D23), https://doi.org/10.1029/2002JD003324

Formenti, P., Elbert, W., Maenhaut, W., Haywood, J., Osborne, S., & Andreae, M. O. (2003). Inorganic and carbonaceous aerosols during the Southern African Regional Science Initiative (SAFARI 2000) experiment: Chemical characteristics, physical properties, and emission data for smoke from African biomass burning. *Journal of Geophysical Research*, *108*(D13), 8488. https://doi.org/10.1029/2002JD002408

Forrister, H., Liu, J., Scheuer, E., Dibb, J., Ziemba, L., Thornhill, K. L., et al. (2015). Evolution of brown carbon in wildfire plumes. *Geophysical Research Letters*, *42*, 4623–4630. https://doi.org/10.1002/2015GL063897

Fromm, M., Alfred, J., Hoppel, K., Hornstein, J., Bevilacqua, R., Shettle, E., et al. (2000). Observations of boreal forest fire smoke in the stratosphere by POAM III, SAGE II, and lidar in 1998. *Journal of Geophysical Research*, *27*(9), 1407–1410. https://doi.org/10.1029/1999GL011200

Garofalo, L. A., Pothier, M. A., Levin, E. J. T., Campos, T., Kreidenweis, S. M., & Farmer, D. K. (2019). Emission and evolution of submicron organic aerosol in smoke from wildfires in the Western United States. *ACS Earth and Space Chemistry*, *3*, 1237–1247.

Gaudichet, A., Echalar, F., Chatenet, B., Quisefit, J. P., Malingre, G., Cachier, H., et al. (1995). Trace elements in tropical African savanna biomass burning aerosols. *Journal of Atmospheric Chemistry*, *22*(1–2), 19–39. https://doi.org/10.1007/BF00708179

Gilman, J. B., Lerner, B. M., Kuster, W. C., Goldan, P. D., Warneke, C., Veres, P. R., et al. (2015). Biomass burning emissions and potential air quality impacts of volatile organic compounds and other trace gases from fuels common in the US. *Atmospheric Chemistry and Physics*, *15*(24), 13,915–13,938. https://doi.org/10.5194/acp-15-13915-2015

Graber, E. R., & Rudich, Y. (2006). Atmospheric HULIS: How humic-like are they? A comprehensive and critical review. *Atmospheric Chemistry and Physics*, *6*, 729–753. https://doi.org/10.5194/acp-6-729-2006

Griffith, D. W. T. (1996). Synthetic calibration and quantitative analysis of gas phase infrared spectra. *Applied Spectroscopy*, *50*, 59–70.

Hammer, M. S., Martin, R. V., van Donkelaar, A., Buchard, V., Torres, O., Ridley, D. A., & Spurr, R. J. D. (2016). Interpreting the ultraviolet aerosol index observed with the OMI satellite instrument to understand absorption by organic aerosols: Implications for atmospheric oxidation and direct radiative effects. *Atmospheric Chemistry and Physics*, *16*, 2507–2523. https://doi.org/10.5194/acp16-2507-2016

Han, Y. M., Cao, J. J., Lee, S. C., Ho, K. F., An, Z. S. (2010). Different characteristics of char and soot in the atmosphere and their ratio as an indicator for source identification in Xi'an, China. *Atmospheric Chemistry and Physics*, *10*(2), 595–607. https://doi.org/10.5194/acp-10-595-2010

Han, Y., Wu, Y., Wang, T., Xie, C., Zhao, K., Zhuang, B., & Li, S. (2015). Characterizing a persistent Asian dust transport event: Optical properties and impact on air quality through the ground-based and satellite measurements over Nanjing, China. *Atmospheric Environment*, *115*, 304–316. https://doi.org/10.1016/j.atmosenv.2015.05.048

Hatch, L. E., Rivas-Ubach, A., Jen, C. N., Lipton, M., Goldstein, A. H., & Barsanti, K. C. (2018). Measurements of I/SVOCs in biomass-burning smoke using solid-phase extraction disks and two-dimensional gas chromatography. *Atmospheric Chemistry and Physics*, *18*, 17,801–17,817. https://doi.org/10.5194/acp-18-17801-2018

Hatch, L. E., Yokelson, R. J., Stockwell, C. E., Veres, P. R., Simpson, I. J., Blake, D. R., et al. (2017). Multi-instrument comparison and compilation of non-methane organic gas emissions from biomass burning and implications for smoke-derived secondary organic aerosol precursors. *Atmospheric Chemistry and Physics*, *17*, 1471–1489. https://doi.org/10.5194/acp-17-1471-2017

Haywood, J. M., Osborne, S. R., Francis, P. N., Keil, A., Formenti, P., Andreae, M. O., Kaye, P. H. (2003). The mean physical and optical properties of regional haze dominated by biomass burning aerosol measured from the C-130 aircraft during SAFARI 2000. *Journal of Geophysical Research: Atmospheres*, *108*(D13), n/a–n/a. https://doi.org/10.1029/2002JD002226

Hecobian, A., Zhang, X., Zheng, M., Frank, N., Edgerton, E. S., & Weber, R. J. (2010). Water-soluble organic aerosol material and the light-absorption characteristics of aqueous extracts measured over the Southeastern United States. *Atmospheric Chemistry and Physics*, *10*, 5965–5977. https://doi.org/10.5194/acp-10-5965-2010

Herron-Thorpe, F. L., Mount, G. H., Emmons, L. K., Lamb, B. K., Jaffe, D. A., Wigder, N. L., et al. (2014). Air quality simulations of wildfires in the Pacific Northwest evaluated with surface and satellite observations during the summers of 2007 and 2008. *Atmospheric Chemistry and Physics*, *14*(22), 12,533–12,551. https://doi.org/10.5194/acp-14-12533-2014

Hodshire, A. L., Bian, Q., Ramnarine, E., Lonsdale, C. R., Alvarado, M. J., Kreidenweis, S. M., et al. (2019). More than emissions and chemistry: Fire size, dilution, and background aerosol also greatly influence near-field biomass burning aerosol aging. *Journal of Geophysical Research: Atmospheres*, *124*, 5589–5611. https://doi.org/10.1029/2018JD029674

Hungershoefer, K., Zeromskiene, K., Iinuma, Y., Helas, G., Trentmann, J., Trautmann, T., et al. (2008). Modeling the optical properties of fresh biomass burning aerosol produced in a smoke chamber: Results from the EFEU campaign. *Atmospheric Chemistry and Physics*, *8*, 3427–3439. https://doi.org/10.5194/acp-8-3427-2008

Iinuma, Y., Böge, O., Gräfe, R., & Herrmann, H. (2010). Methylnitrocatechols: Atmospheric tracer compounds for biomass burning secondary organic aerosols. *Environmental Science & Technology*, *44*, 8453–8459. https://doi.org/10.1021/es102938a

Jacob, D. J., Crawford, J. H., Maring, H., Clarke, A. D., Dibb, J. E., Emmons, L. K., et al. (2010). The Arctic Research of the Composition of the Troposphere from Aircraft and Satellites (ARCTAS) mission: Design, execution, and first results. *Atmospheric Chemistry and Physics*, *10*, 5191–5212. https://doi.org/10.5194/acp-10-5191-2010

Jacobson, M. Z. (2014). Effects of biomass burning on climate, accounting for heat and moisture fluxes, black and brown carbon, and cloud absorption effects. *Journal of Geophysical Research: Atmospheres*, *119*, 8980–9002. https://doi.org/10.1002/2015JD021861

Jaffe, D. A., Cooper, O. R., Fiore, A. M., Henderson, B. H., Gail, S., Russell, A. G., et al. (2018). Scientific assessment of background ozone over the U.S.: Implications for air quality management. *Elementa: Science of the Anthropocene*, *6*, 56. https://doi.org/10.1525/elementa.309

Jaffe, D. A., Wigder, N., Downey, N., Pfister, G., Boynard, A., & Reid, S. B. (2013). Impact of wildfires on ozone exceptional events in the western U.S. *Environmental science & technology*, *47*(19), 11,065–11,072. https://doi.org/10.1021/es402164f

Jen, C. N., Hatch, L. E., Selimovic, V., Yokelson, R. J., Weber, R., Fernandez, A. E., et al. (2019). Speciated and total emission factors of particulate organics from burning western US wildland fuels and their dependence on combustion efficiency. *Atmospheric Chemistry and Physics*, *19*(2), 1013–1026. https://doi.org/10.5194/acp-19-1013-2019

Jethva, H., & Torres, O. (2011). Satellite-based evidence of wavelength-dependent aerosol absorption in biomass burning smoke inferred from ozone monitoring instrument. *Atmospheric Chemistry and Physics*, *11*(20), 10,541–10,551. https://doi.org/10.5194/acp-11-10541-2011

Jiang, H., & Feingold, G. (2006). Effect of aerosol on warm convective clouds: aerosol-cloud-surface flux feedbacks in a new coupled large eddy model. *Journal Geophysical Research*, *111*, D01202. https://doi.org/10.1029/2005JD006138

Jolly, W. M., Cochrane, M. A., Freeborn, P. H., Holden, Z. A., Brown, T. J., Williamson, G. J., & Bowman, D. M. J. S. (2015). Climate-induced variations in global wildfire danger from 1979 to 2013. *Nature Communications*, *6*, 7537. https://doi.org/10.1038/ncomms8537

Kolusu, S. R., Marsham, J. H., Mulcahy, J., Johnson, B., Dunning, C., Bush, M., & Spracklen, D. V. (2015). Impacts of Amazonia biomass burning aerosols assessed from short-range weather forecasts. *Atmospheric Chemistry and Physics*, *15*, 12,251–12,266. https://doi.org/10.5194/acp-15-12251-2015

Koss, A. R., Sekimoto, K., Gilman, J. B., Selimovic, V., Coggon, M. M., Zarzana, K. J., et al. (2018). Non-methane organic gas emissions from biomass burning: Identification, quantification, and emission factors from PTR-ToF during the FIREX 2016 laboratory experiment. *Atmospheric Chemistry and Physics*, *18*(5), 3299–3319. https://doi.org/10.5194/acp-18-3299-2018

Lack, D. A., & Cappa, C. D. (2010). Impact of brown and clear carbon on light absorption enhancement, single scatter albedo and absorption wavelength dependence of black carbon. *Atmospheric Chemistry and Physics*, *10*(9), 4207–4220. https://doi.org/10.5194/acp-10-4207-2010

Lack, D. A., Cappa, C. D., Covert, D. S., Baynard, T., Massoli, P., Sierau, B., et al. (2008). Bias in filter based aerosol light absorption measurements due to organic aerosol loading: Evidence from ambient measurements. *Aerosol Science and Technology*, *42*, 1033–1041. https://doi.org/10.1080/02786820802389285

Lack, D. A., & Langridge, J. M. (2013). On the attribution of black and brown carbon light absorption using the Ångström exponent. *Atmospheric Chemistry and Physics*, *13*, 10,535–10,543. https://doi.org/10.5194/acp-13-10535-2013

Laskin, A., Laskin, J., & Nizkorodov, S. A. (2015). Chemistry of atmospheric brown carbon. *Chemical Reviews*, *115*(10), 4335–4382. https://doi.org/10.1021/cr5006167

Lee, J. D., Moller, S. J., Read, K. A., Lewis, A. C., Mendes, L., & Carpenter, L. J. (2009). Year-round measurements of nitrogen oxides and ozone in the tropical North Atlantic marine boundary layer. *Journal of Geophysical Research*, *114*, D21302. https://doi.org/10.1029/2009JD011878

Lewis, K., Arnott, W. P., Moosmuller, H., & Wold, C. E. (2008). Strong spectral variation of biomass smoke light absorption and single scattering albedo observed with a novel dual-wavelength photoacoustic instrument. *Journal of Geophysical Research*, *113*, D16203. https://doi.org/10.1029/2007JD009699

Li, H., Lamb, K. D., Schwarz, J. P., Selimovic, V., Yokelson, R. J., McMeeking, G. R., May, A. A. (2019). Inter-comparison of black carbon measurement methods for simulated open biomass burning emissions. *Atmospheric Environment*, *206*, 156–169. https://doi.org/10.1016/j.atmosenv.2019.03.010

Li, Y., & Shiraiwa, M. (2019). Timescales of secondary organic aerosols to reach equilibrium at various temperatures and relative humidities. *Atmospheric Chemistry and Physics*, *19*, 5959–5971. https://doi.org/10.5194/acp-19-5959-2019

Lim, C. Y., Hagan, D. H., Coggon, M. M., Koss, A. R., Sekimoto, K., de Gouw, J., et al. (2019). Secondary organic aerosol formation from the laboratory oxidation of biomass burning emissions. *Atmospheric Chemistry and Physics*, *19*(19), 12,797–12,809. https://doi.org/10.5194/acp-19-12797-2019

Lindaas, J., Farmer, D. K., Pollack, I. B., Abeleira, A., Flocke, F., Roscioli, R., et al. (2017). Changes in ozone and precursors during two aged wildfire smoke events in the Colorado Front Range in summer 2015. *Atmospheric Chemistry and Physics*, *17*, 10,691–10,707. https://doi.org/10.5194/acp-17-10691-2017

Liu, C., Chung, C. E., Yin, Y., & Schnaiter, M. (2018). The absorption Ångström exponent of black carbon: From numerical aspects. *Atmospheric Chemistry and Physics*, *18*(9), 6259–6273. https://doi.org/10.5194/acp-18-6259-2018

Liu, J., Scheuer, E., Dibb, J., Ziemba, L. D., Thornhill, K. L., Anderson, B. E., et al. (2014). Brown carbon in the continental troposphere. *Geophysical Research Letters*, *41*, 2191–2195. https://doi.org/10.1002/2013GL058976

Liu, X., Huey, G. L., Yokelson, R. J., Selimovic, V., Simpson, I. J., Müller, M., et al. (2017). Airborne measurements of western U. S wildfire emissions: Comparison with prescribed burning and air quality implications. *Journal of Geophysical Research: Atmospheres*, *122*, 6108–6129. https://doi.org/10.1002/2016JD026315

Liu, X., Zhang, Y., Huey, L. G., Yokelson, R. J., Wang, Y., Jimenez, J. L., et al. (2016). Agricultural fires in the southeastern U.S. during SEAC⁴RS: Emissions of trace gases and particles and evolution of ozone, reactive nitrogen, and organic aerosol. *Journal of Geophysical Research: Atmospheres*, *121*, 7383–7414. https://doi.org/10.1002/2016JD025040

Mardi, A. H., Dadashazar, H., MacDonald, A. B., Braun, R. A., Crosbie, E., Xian, P., et al. (2018). Biomass burning plumes in the vicinity of the California coast: Airborne characterization of physiochemical properties, heating rates, and spatiotemporal features. *Journal of Geophysical Research: Atmospheres*, *123*, 13,560–13,582. https://doi.org/10.1029/2018JD029134

Marlon, J. R., Bartlein, P. J., Gavin, D. G., Long, C. J., Anderson, R. S., Briles, C. E., et al. (2012). Long-term perspective on wildfires in the western USA. *Proceedings of the National Academy of Sciences*, *109*(9), E535–E543. https://doi.org/10.1073/pnas.1112839109

Maudlin, L. C., Wang, Z., Jonsson, H. H., & Sorooshian, A. (2015). Impact of wildfires on size-resolved aerosol composition at a coastal California site. *Atmospheric Environment*, *119*, 59–68. https://doi.org/10.1016/j.atmosenv.2015.08.039

May, A. A., Lee, T., McMeeking, G. R., Akagi, S., Sullivan, A. P., Urbanski, S., et al. (2015). Observations and analysis of organic aerosol evolution in some prescribed fire smoke plumes. *Atmospheric Chemistry and Physics*, *15*, 6323–6335. https://doi.org/10.5194/acp-15-6323-2015

May, A. A., Levin, E. J. T., Hennigan, C. J., Riipinen, I., Lee, T., Collett, J. L. Jr., et al. (2013). Gas-particle partitioning of primary organic aerosol emissions: 3. Biomass burning. *Journal of Geophysical Research: Atmospheres*, *118*, 11,327–11,338. https://doi.org/10.1002/jgrd.50828

May, A. A., McMeeking, G. R., Lee, T., Taylor, J. W., Craven, J. S., Burling, I., et al. (2014). Aerosol emissions from prescribed fires in the United States: A synthesis of laboratory and aircraft measurements. *Journal of Geophysical Research: Atmospheres*, *119*, 11,826–11,849. https://doi.org/10.1002/2014JD021848

McClure, C. D., & Jaffe, D. A. (2018). Investigation of high ozone events due to wildfire smoke in an urban area. *Atmospheric Environment*, *194*, 146–157. https://doi.org/10.1016/j.atmosenv.2018.09.021

McComiskey, A., Schwartz, S. E., Schmid, B., Guan, H., Lewis, E. R., Ricchiazzi, P., & Ogren, J. A. (2008). Direct aerosol forcing: Calculation from observables and sensitivities to inputs. *Journal of Geophysical Research*, *113*. https://doi.org/10.1029/2007JD009170

Mohr, C., Lopez-Hilfiker, F., Zotter, P., Prévôt, A. S. H., Xu, L., Ng, N. L., et al. (2013). Contribution of nitrated phenols to wood burning brown carbon light absorption in Detling, United Kingdom during winter time. *Environmental Science & Technology*, *47*, 6316–6324. https://doi.org/10.1021/es400683v

Morgan, W. T., Allan, J. D., Bauguitte, S., Darbyshire, E., Flynn, M. J., Lee, J., et al. (2020). Transformation and aging of biomass burning carbonaceous aerosol over tropical South America from aircraft in-situ measurements during SAMBBA. *Atmospheric Chemistry and Physics Discussions*, *20*, 5309–5326. https://doi.org/10.5194/acp-20-5309-2020

Morris, G. A., Hersey, S., Thompson, A. M., Paweson, S., Nielsen, J. E., Colarco, P. R., et al. (2006). Alaskan and Canadian forest fires exacerbate ozone pollution over Houston, Texas, on 19 and 20 July 2004. *Journal of Geophysical Research*, *111*, D24S03. https://doi.org/10.1029/2006JD007090

Nakayama, T., Suzuki, H., Kagamitani, S., & Ikeda, Y. (2015). Characterization of a three wavelength Photoacoustic Soot Spectrometer (PASS-3) and a Photoacoustic Extinctiometer (PAX). *Journal of the Meteorological Society of Japan*, *93*, 285–308. https://doi.org/10.2151/jmsj.2015-016

Nergui, T., Lee, Y., Chung, S. H., Lamb, B. K., Yokelson, R. J., & Barsanti, K. (2017). *Integrating measurement based new knowledge on wildland fire emissions and chemistry into the AIRPACT air quality forecasting for the Pacific Northwest*. New Orleans, LA: American Geophysical Union Fall Meeting. Abstract# A41L-06

Palm, B. B., Campuzano-Jost, P., Day, D. A., Ortega, A. M., Fry, J. L., Brown, S. S., et al. (2017). Secondary organic aerosol formation from in situ OH, O_3, and NO_3 oxidation of ambient forest air in an oxidation flow reactor. *Atmospheric Chemistry and Physics*, *17*, 5331–5354. https://doi.org/10.5194/acp-17-5331-2017

Peterson, D., Fromm, M. D., Solbrig, J. E., Hyer, E. J., Surratt, M. L., & Campbell, J. R. (2017). Detection and inventory of intense pyro-convection in Western North America using *GOES-15* daytime infrared data. *American Meteorological Society*, *56*, 471–493. https://doi.org/10.1175/JAMC-D-16-0226.1

Pokhrel, R. P., Beamesderfer, E. R., Wagner, N. L., Langridge, J. M., Lack, D. A., Jayarathne, T., et al. (2017). Relative importance of black carbon, brown carbon, and absorption enhancement from clear coatings in biomass burning emissions. *Atmospheric Chemistry and Physics*, *17*(8), 5063–5078. https://doi.org/10.5194/acp-17-5063-2017

Pokhrel, R. P., Wagner, N. L., Langridge, J. M., Lack, D. A., Jayarathne, T., Stone, E. A., et al. (2016). Parameterization of single-scattering albedo (SSA) and absorption Ångström exponent (AAE) with EC/OC for aerosol emissions from biomass burning. *Atmospheric Chemistry and Physics*, *16*(15), 9549–9561. https://doi.org/10.5194/acp-16-9549-2016

Praveen, P. S., Ahmed, T., Kar, A., Rehman, I. H., & Ramanathan, V. (2012). Link between local scale BC emissions and large scale atmospheric solar absorption. *Atmospheric Chemistry and Physics*, *12*, 1173–1187. https://doi.org/10.5194/acp-12-1173-2012

Reid, J. S., Koppmann, R., Eck, T. F., & Eleuterio, D. P. (2005). A review of biomass burning emissions, Part II: Intensive physical properties of biomass burning particles. *Atmospheric Chemistry and Physics*, *5*, 799–825. https://doi.org/10.5194/acp-5-799-2005

Robinson, A. L., Donahue, N. M., Shrivastava, M. K., Weitkamp, E. A., Sage, A. M., Grieshop, A. P., et al. (2007). Rethinking organic aerosols: Semivolatile emissions and photochemical aging. *Science*, *315*, 1259–1262. https://doi.org/10.1126/science.1133061

Rothman, L. S., Gordon, I. E., Barbe, A., Benner, D. C., Bernath, P. F., Birk, M., et al. (2009). The HITRAN 2008 molecular spectroscopic database. *Journal of Quantitative Spectroscopy and Radiative*, *110*, 533–572. https://doi.org/10.1016/j.jqsrt.2009.02.013

Russell, P. B., Bergstrom, R. W., Shinozuka, Y., Clarke, A. D., DeCarlo, P. F., Jimenez, J. L., et al. (2010). Absorption angstrom exponent in AERONET and related data as an indicator of aerosol composition. *Atmospheric Chemistry & Physics Discussions*, *10*, 1155–1169. https://doi.org/10.5194/acp-10-1155-2010

Sahu, L. K., Kondo, Y., Moteki, N., Takegawa, N., Zhao, Y., Cubison, M. J., et al. (2012). Emission characteristics of black carbon in anthropogenic and biomass burning plumes over California during ARCTAS-CARB 2008. *Journal of Geophysical Research*, *117*, D16302. https://doi.org/10.1029/2011JD017401

Saide, P. E., Peterson, D. A., da Silva, A., Anderson, B., Ziemba, L. D., Diskin, G., et al. (2015). Revealing important nocturnal and day-to-day variations in fire smoke emissions through a multiplatform inversion. *Geophysical Research Letters*, *42*, 3609–3618. https://doi.org/10.1002/2015GL063737

Saleh, R., Robinson, E. S., Tkacik, D. S., Ahern, A. T., Liu, S., Aiken, A. C., et al. (2014). Brownness of organics in aerosols from biomass burning linked to their black carbon content. *Nature Geoscience*, *7*(9), 647–650. https://doi.org/10.1038/ngeo2220

Santín, C., Doerr, S. H., Preston, C. M., & Gonzalez-Rodriguez, G. (2015). Pyrogenic organic matter production from wildfires: A missing sink in the global carbon cycle. *Global Change Biology*, *21*(4), 1621–1633. https://doi.org/10.1111/gcb.12800

Schlosser, J. S., Braun, R. A., Bradley, T., Dadashazar, H., MacDonald, A. B., Aldhaif, A. A., et al. (2017). Analysis of aerosol composition data for western United States wildfires between 2005 and 2015: Dust emissions, chloride depletion, and most enhanced aerosol constituents. *Journal of Geophysical Research: Atmospheres*, *122*, 8951–8966. https://doi.org/10.1002/2017JD026547

Schoennagel, T., Balch, J. K., Brenkert-Smith, H., Dennison, P. E., Harvey, B. J., Krawchuk, M. A., et al. (2017). Adapt to more wildfire in western North American forests as climate changes. *Proceedings of the National Academy of Sciences*, *114*, 4582–4590. https://doi.org/10.1073/pnas.1617464114

Sedlacek, A. J. III, Buseck, P. R., Adachi, K., Onasch, T. B., Springston, S. R., & Kleinman, L. (2018). Formation and evolution of tar balls from northwestern US wildfires. *Atmospheric Chemistry and Physics*, *18*(15), 11,289–11,301. https://doi.org/10.5194/acp-18-11289-2018

Selimovic, V., Yokelson, R. J., McMeeking, G. R., & Coefield, S. (2019). In situ measurements of trace gases, PM, and aerosol optical properties during the 2017 NW US wildfire smoke event. *Atmospheric Chemistry and Physics*, *19*(6), 3905–3926. https://doi.org/10.5194/acp-19-3905-2019

Selimovic, V., Yokelson, R. J., Warneke, C., Roberts, J. M., de Gouw, J., Reardon, J., & Griffith, D. W. T. (2018). Aerosol optical properties and trace gas emissions by PAX and OP-FTIR for laboratory-simulated western US wildfires during FIREX. *Atmospheric Chemistry and Physics*, *18*(4), 2929–2948. https://doi.org/10.5194/acp-18-2929-2018

Shaddix, C. R., Harrington, J. E., & Smyth, K. C. (1994). Quantitative measurements of enhanced soot production in a flickering methane/air diffusion flame. *Combustion and Flame*, *99*(3–4), 723–732. https://doi.org/10.1016/0010-2180(94)90067-1

Shingler, T., Crosbie, E., Ortega, A., Shiraiwa, M., Zuend, A., Beyersdorf, A., et al. (2016). Airborne characterization of subsaturated aerosol hygoscopicity and dry refractive index from the surface to 6.5 km during the SEAC4RS campaign. *Journal of Geophysical Research: Atmospheres*, *121*, 4188–4210. https://doi.org/10.1002/2015JD024498

Shivdenko, A. Z., & Schepaschenko, D. G. (2013). Climate change and wildfires in Russia. *Contemporary Problems of Ecology*, *6*, 683–692. https://doi.org/10.1134/S199542551307010X

Stein, A. F., Draxler, R. R., Rolph, G. D., Stunder, B. J. B., Cohen, M. D., & Ngan, F. (2015). NOAA's HYSPLIT atmospheric transport and dispersion modeling system. *Bulletin of the American Meteorological Society*, *96*(12), 2059–2077. https://doi.org/10.1175/BAMS-D-14-00110.1

Stevens, J. T., Safford, H. G., & Latimer, A. M. (2014). Wildfire-contigent effects of fuel treatments can promote ecological resilience in seasonally dry conifer forests. *Canadian Journal of Forest Research*, *44*(8), 843–854. https://doi.org/10.1139/cjfr-2013-0460

Stocks, B. J., van Wilgen, B. W., Trollope, W. S. W., McRae, D. J., Mason, J. A., Weirich, F., & Potgieter, A. L. F. (1996). Fuels and fire behavior dynamics on large-scale savanna fires in Kruger National Park, South Africa. *Journal of Geophysical Research*, *101*(D19), 23,541–23,550.

Stockwell, C. E., Christian, T. J., Goetz, J. D., Jayarathne, T., Bhave, P. V., Praveen, P. S., et al. (2016). Nepal Ambient Monitoring and Source Testing Experiment (NAMaSTE): Emissions of trace gases and light-absorbing carbon from wood and dung cooking fires, garbage and crop residue burning, brick kilns, and other sources. *Atmospheric Chemistry and Physics*, *16*(17), 11,043–11,081. https://doi.org/10.5194/acp-16-11043-2016

Stockwell, C. E., Jayarathne, T., Cochrane, M. A., Ryan, K. C., Putra, E. I., Saharjo, B. H., et al. (2016). Field measurements of trace gases and aerosols emitted by peat fires in Central Kalimantan, Indonesia, during the 2015 El Niño. *Atmospheric Chemistry and Physics*, *16*(18), 11,711–11,732. https://doi.org/10.5194/acp-16-11711-2016

Stockwell, C. E., Veres, P. R., Williams, J., & Yokelson, R. J. (2015). Characterization of biomass burning emissions from cooking fires, peat, crop residue, and other fuels with high-resolution proton-transfer-reaction time-of-flight mass spectrometry. *Atmospheric Chemistry and Physics*, *15*(2), 845–865. https://doi.org/10.5194/acp-15-845-2015

Subramanian, R., Roden, C. A., Boparai, P., & Bond, T. C. (2007). Yellow beads and missing particles: Trouble ahead for filter-based absorption measurements. *Aerosol Science and Technology*, *41*, 630–637. https://doi.org/10.1080/02786820701344589

Thornhill, G. D., Ryder, C. L., Highwood, E. J., Shaffrey, L. C., & Johnson, B. T. (2018). The effect of South American biomass burning aerosol emissions on the regional climate. *Atmospheric Chemistry and Physics*, *18*, 5321–5342. https://doi.org/10.5194/acp-18-5321-2018

Tkacik, D. S., Robinson, E. S., Ahern, A., Saleh, R., Stockwell, C., Veres, P., et al. (2017). A dual-chamber enhancement method for quantifying effects of atmospheric perturbations on secondary organic aerosol formation from biomass burning emissions. *Journal of Geophysical Research: Atmospheres*, *122*(11), 6043–6058. https://doi.org/10.1002/2016JD025784

Tomaz, S., Cui, T., Chen, Y., Sexton, K. G., Roberts, J. M., Warneke, C., et al. (2018). Photochemical cloud processing of primary wildfire emissions as a potential source of secondary organic aerosol. *Environmental Science & Technology*, *52*(19), 11,027–11,037. https://doi.org/10.1021/acs.est.8b03293

Turner, M. G., Braziunas, K. H., Hansen, W. D., & Harvey, B. J. (2019). Short-interval severe fire erodes the resilience of subalpine Lodgepole pine forest. *Proceedings of the National Academy of Sciences USA*, *116*(23), 11,319–11,328. https://doi.org/10.1073/pnas.1902841116

United States Department of Agriculture. (2015). The rising cost of wildfire operations: Effects on the forest service's non-fire work. https://www.fs.fed.us/sites/default/files/2015-Fire-Budget-Report.pdf

Vakkari, V., Beukes, J. P., Dal Maso, M., Aurela, M., Josipovic, M., & van Zyl, P. G. (2018). Major secondary aerosol formation in southern African open biomass burning plumes. *Nature Geoscience*, *11*(8), 580–583. https://doi.org/10.1038/s41561-018-0170-0

Vermote, E., Ellicott, E., Dubovik, O., Lapyonok, T., Chin, M., Giglio, L., Roberts, G. J. (2009). An approach to estimate global biomass burning emissions of organic and black carbon from MODIS fire radiative power. *Journal of Geophysical Research*, *114*(D18), https://doi.org/10.1029/2008JD011188

Wagenbrenner, N. S., Forthofer, J. M., Lamb, B. K., Shannon, K. S., & Butler, B. W. (2016). Downscaling surface wind predictions from numerical weather prediction models in complex terrain with WindNinja. *Atmospheric Chemistry and Physics*, *16*, 5229–5241. https://doi.org/10.5194/acp-16-5229-2016

Wang, J., Geng, N. B., Xu, Y. F., Zhang, W. D., Tang, X. Y., & Zhang, R. Q. (2014). PAHs in PM2.5 in Zhengzhou: Concentration, carcinogenic risk analysis and source apportionment. *Environmental Monitoring and assessment*, *186*(11), 7461–7473. https://doi.org/10.1007/s10661-014-3940-1

Wang, J., Yue, Y., Wang, Y., Ichoku, C., Ellison, L., & Zeng, J. (2017). Mitigating satellite-bassed fire sampling limitations in deriving biomass burning emission rates: Application to WRF-Chem model over the northern sub-saharan African region. *Journal of Geophysical Research: Atmospheres*, *123*, 507–528. https://doi.org/10.1002/2017JD026840

Westerling, A. L., Hidalgo, H. G., Cayan, D. R., & Swetnam, T. W. (2006). Warming and earlier spring increase western US forest wildfire activity. *Science*, *313*, 940–943. https://doi.org/10.1126/science.1128834

Xu, J., Zhang, Q., Shi, J., Ge, X., Xie, C., Wang, J., et al. (2018). Chemical characteristics of submicron particles at the central Tibetan Plateau: Insights from aerosol mass spectrometry. *Atmospheric Chemistry and Physics*, *18*(1), 427–443. https://doi.org/10.5194/acp-18-427-2018

Yokelson, R. J., Andreae, M. O., & Akagi, S. K. (2013). Pitfalls with the use of enhancement ratios or normalized excess mixing ratios measured in plumes to characterize pollution sources and aging. *Atmospheric Measurement Techniques*, *6*, 2155–2158. https://doi.org/10.5194/amt-6-2155-2013

Yokelson, R. J., Christian, T. J., Karl, T. G., & Guenther, A. (2008). The tropical forest and fire emissions experiment: Laboratory fire measurements and synthesis of campaign data. *Atmospheric Chemistry and Physics*, *8*(13), 3509–3527. https://doi.org/10.5194/acp-8-3509-2008

Yokelson, R. J., Crounse, J. D., DeCarlo, P. F., Karl, T., Urbanski, S., Atlas, E., et al. (2009). Emissions from biomass burning in the Yucatan. *Atmospheric Chemistry and Physics*, *9*, 5785–5812. https://doi.org/10.5194/acp-9-5785-2009

Yokelson, R. J., Goode, J. G., Ward, D. E., Susott, R. A., Babbitt, R. E., Wade, D. D., et al. (1999). Emissions of formaldehyde, acetic acid, methanol, and other trace gases from biomass fires in North Carolina measured by airborne Fourier transform infrared spectroscopy. *Journal of Geophysical Research*, *104*(D23), 30109–30125. https://doi.org/10.1029/1999JD900817

Yokelson, R. J., Karl, T., Artaxo, P., Blake, D. R., Christian, T. J., Griffith, D. W. T., et al. (2007). The tropical forest and fire emissions experiment: Overview and airborne fire emission factor measurements. *Atmospheric Chemistry and Physics*, *7*(19), 5175–5196. https://doi.org/10.5194/acp-7-5175-2007

Zhang, A., Wang, Y., Zhang, Y., Weber, R. J., Song, Y., Ke, Z., & Zou, Y. (2020). Modeling the global radiative effect of brown carbon: A potentially larger heating source in the tropical free troposphere than black carbon. *Atmospheric Chemistry and Physics*, *20*, 1901–1920. https://doi.org/10.5194/acp-20-1901-2020

Zhou, S., Collier, S., Jaffe, D. A., Briggs, N. L., Hee, J., Sedlacek, A. J. III, et al. (2017). Regional influence of wildfires on aerosol chemistry in the western US and insights into atmospheric aging of biomass burning organic aerosol. *Atmospheric Chemistry and Physics*, *17*, 2477–2493. https://doi.org/10.5194/acp-17-2477-2017